

A coupled level set and volume of fluid method on unstructured grids for the direct numerical simulations of two-phase flows including phase change

Nikhil Kumar Singh, B. Premachandran*

Department of Mechanical Engineering, Indian Institute of Technology Delhi, New Delhi 110 016, India



ARTICLE INFO

Article history:

Received 18 September 2017

Received in revised form 16 January 2018

Accepted 19 January 2018

Keywords:

Volume of fluid

Level set

CLSOVF

Film boiling

Unstructured grid

ABSTRACT

In the present study, a coupled level set and volume of fluid (CLSOVF) method is developed for two-dimensional unstructured grids to perform direct numerical simulations of two-phase flows including phase change. The volume fraction is advected using a multi-directional advection algorithm, where the flux polygons are constructed using vertex velocities and a scaling factor based on cell face velocities is used to correct the advected volume fraction. The level set field is advected using a total variational diminishing (TVD) scheme and geometrically reinitialized at the end of each time step. The performance of the proposed CLSOVF method is evaluated in detail on unstructured grids, both qualitatively and quantitatively, prior to simulation of phase change problems. A number of advection test cases and two-phase flow problems are considered for this purpose. Results obtained for film boiling over a horizontal flat plate using an unstructured grid show excellent agreement with results available in the literature. The numerical study of natural convection film boiling over a horizontal cylinder at different wall superheats shows a better agreement with semi-empirical correlations compared to other available numerical results.

© 2018 Published by Elsevier Ltd.

1. Introduction

Phase change phenomena like boiling are characterized by high heat transfer rates and thus find applications in a plethora of fields such as power generation, refrigeration, nuclear reactors, and electronics cooling. Sustained efforts towards understanding the flow physics and heat transfer associated with different regimes of boiling is thus of fundamental importance. In the second half of the twentieth century, boiling was the subject of many experimental and analytical studies. Experiments have provided numerous correlations to predict boiling characteristics under different regimes for specific geometries. On the other hand, theoretical studies involve several assumptions pertaining to aspects such as vapor and fluid properties, and surface tension. Nevertheless these studies have immensely improved our understanding of boiling, and would continue as we look for further insights. With the rapid and massive advancements in the field of computational fluid dynamics over the last few decades, it was imperative that numerical techniques would be developed to model two-phase flows including phase change phenomena such as boiling. Moreover, as

noted by pioneers in this field [1–3], the small spatial and temporal scales associated with the physics of boiling make experimental measurements very difficult, and computations of boiling flows would help to uncover aspects that may still not be well understood.

Two-phase flows can be modelled using Euler-Euler model, which requires a priori information to a certain extent about the interfacial transport processes [4]. Direct numerical simulations of two-phase flows avoid any empiricism by identifying the sharp interface and solving the transport mechanisms directly across the interface. Surface tension between the two phases thus becomes an important factor that affects the interface shape. Keeping track of the interface position with time, an abrupt change in properties across the sharp interface, and non-linear surface tension force render these numerical simulations quite challenging.

The methods predominantly used presently for direct numerical simulation of two-phase flows are the volume-of-fluid (VOF) method, the level set (LS) method, the coupled level set and volume-of-fluid (CLSOVF) method, and the front tracking method. The front tracking method involves solution of transport equations on a fixed grid while utilizing a moving grid for tracking the interface. The front tracking approach for incompressible multi-fluid flows developed by Unverdi and Tryggvason [5], was extended

* Corresponding author.

E-mail address: prem@mech.iitd.ac.in (B. Premachandran).

Nomenclature

| | |
|----------------|------------------------------------------------------|
| c_p | specific heat at constant pressure (J/kg K) |
| F | volume fraction or colour function |
| F_{st} | volumetric surface tension force (N/m ³) |
| g | acceleration due to gravity (m/s ²) |
| H | smoothed Heaviside function |
| h_{lv} | latent heat of vaporization (J/kg) |
| k | thermal conductivity (W/m K) |
| \dot{m} | mass flux across interface (kg/m ² s) |
| \mathbf{n} | interfacial unit normal vector |
| Nu | Nusselt number |
| P | pressure (Pa) |
| $\mathbf{q''}$ | heat flux vector (W/m ²) |
| S | surface area (m ²) |
| t | time (s) |
| T | temperature (K) |
| u, v | velocity components in x and y coordinates (m/s) |
| \mathbf{V} | cell velocity vector (m/s) |

Greek symbols

| | |
|-------------|-------------------------------------------|
| κ | interfacial curvature (m ⁻¹) |
| μ | dynamic viscosity (N s/m ²) |
| ρ | density (kg/m ³) |
| σ | surface tension coefficient (N/m) |
| ϕ | level set function |
| λ_0 | characteristic capillary length scale (m) |

Subscripts

| | |
|-----|--------------|
| int | interface |
| l | liquid phase |
| v | vapor phase |
| sat | saturation |

for boiling flows by Juric and Tryggvason [2]. The other methods mentioned above capture the interface on an Eulerian grid, and are thus classified as interface capturing methods. This can arguably be the reason for a lower computational complexity leading to their wider use.

The VOF method uses a colour function with a value of 0 or 1 in either of the two phases, while having an intermediate value at the interface cells, representing the volume fraction of one of the phases in each cell. VOF methods either use high resolution schemes to advect the interface or involve geometrical interface advection and reconstruction. The former method usually leads to a diffused interface. Hence, the geometrical approach is more popular. Welch and Wilson [3] used the VOF method with Young's piecewise linear interface calculation (PLIC) scheme [6] to simulate horizontal film boiling. The mass conservation implicit within the VOF method has kept it relevant and widely in use till date. However, a major drawback is the generation of spurious currents due to inaccurate calculation of interface curvature, since it is based on the discrete colour function distribution. Several improvements have subsequently been proposed for two-phase flows on structured uniform grids, which focus on improved interface reconstruction techniques and accurate surface tension calculation [7–10]. However, the applicability, performance, computational cost and complexity of many of these methods on non-orthogonal or unstructured grids is not well-established or reported.

The VOF-PLIC schemes still remain the most popular choice for interface reconstruction. Height function (HF) method for estimating curvature from volume fractions has been reported [11,12] to provide second-order accurate results on structured grids, and its implementation is also easier than parabolic or spline interface reconstruction [13]. However, studies have also revealed that HF method which uses a fixed stencil of cells may lead to poor results in regions where the curvature is not adequately resolved by grid size [11,12] and the spurious currents are sensitive to errors in the VOF transport scheme [14]. HF method has been implemented on unstructured grids in a few studies [15,16]. However, detailed investigations of these methods for different practical problems is yet to emerge. To reduce spurious currents, some of the studies have also highlighted the need for an algorithm to balance the pressure and surface tension forces in the vicinity of the interface [12,17,18].

Another aspect of VOF methods covered in several studies [9,17,19,20] is the unsplit or multi-dimensional advection of the colour function, which as opposed to operator split advection does

not require advection in each coordinate direction separately for every time step. This not only reduces computational time but also makes the use of VOF methods feasible for irregular or complex geometries with unstructured grids.

After Welch and Wilson [3], several researchers have used VOF framework for simulation of film boiling, for which the reader may refer to the review by Kharangane and Mudawar [21]. Recently, Tsui and Lin proposed a modified VOF method [22] applicable to unstructured grids requiring successive corrections of colour function value at a given time step. The performance of the method on unstructured grids is shown only qualitatively for two advection test cases, while other two-phase flow results are presented only for structured grids. Tsui et al. [23] used the above method to simulate two-dimensional film boiling over a flat plate and a horizontal cylinder. Recently, Tsui and Lin [24] extended their method for three-dimensional simulation of film boiling over a flat plate using a structured grid. Ding et al. [25] presented a VOF based method for phase change problems using an energy source donor-acceptor scheme to suppress the numerical oscillations resulting from different factors in such simulations.

Level set (LS) methods form another important class of interface capturing methods originating from the work of Osher and Sethian [26] and further developed by Sussman et al. [27]. The LS methods use a signed distance function that takes positive values of distance from the interface in one of the phases, negative in the other, while the zero contour represents the interface. The LS advection equation is solved directly with appropriate discretization schemes without any complex geometric tasks as employed in VOF methods. Hence, an extension of the LS method to three dimensions or unstructured grids is relatively easier. The curvature and surface tension can be calculated accurately from the smooth distribution of the LS function. However, the LS function does not remain a smooth signed distance function as it advects over time and also inherently suffers from mass conservation errors. To maintain it to be a smooth signed distance function, reinitialization of the LS function at each time step proposed by Sussman et al. [27] is widely used. Still, the reinitialization procedure leads to mass errors further compounded during interface evolution. Subsequent improvements to the LS method deal with the mass errors and are highlighted in the work of Gada and Sharma [28]. Another development is the use of ghost fluid method [29] in conjunction with the LS method for sharp interface simulations. Son and Dhir [1,30] first used the LS method to simulate film boiling on horizontal surfaces,

and later used it in conjunction with the ghost fluid method to simulate two and three-dimensional film boiling on a horizontal cylinder [31,32]. Gada and Sharma [28] used a dual grid LS method and studied two-phase flow problems including two-dimensional saturated film boiling of water over a flat plate.

A non-trivial but obvious outcome of the observations from VOF and LS methods was the coupling of the two to eliminate mass errors along with accurate surface tension estimation. This led to the development of coupled level set and volume of fluid (CLSVOF) method [33,34], where the smooth LS function is used to estimate curvature and surface tension while the VOF scheme ensures exact mass conservation. Over the recent years, CLSVOF method has evolved as an important approach for two-phase flow modelling with several studies [35–40] demonstrating its ability to predict interfacial phenomena. Tomar et al. [38] used CLSVOF method for simulating horizontal film boiling of water and R134a with different wall superheats. Gerlach et al. [39] compared CLSVOF method with PROST [8] and a volume fraction smoothing method for surface tension calculation, and observed that CLSVOF method provides a good alternative to the computationally intensive PROST scheme. Welch and Biswas [41] and Tomar et al. [42] further included the effect of electric field on film boiling in conjunction with CLSVOF method. However, as noted by Ningegowda and Premachandran [40], all the above CLSVOF methods for two-phase flows including that used by Tomar et al. [38] for phase change, except Yang et al. [43], employed operator split advection. This restricted the use of CLSVOF technique to structured grids, at the same time making it computationally expensive since the interface reconstruction procedures had to be carried out twice and thrice for 2D and 3D problems respectively.

Ningegowda and Premachandran [40] proposed a CLSVOF method with multi-directional advection, using the EMFPA VOF advection of López et al. [9] for two-phase problems including phase change. They implemented the procedure for structured uniform and non-uniform grids, and studied two-dimensional horizontal film boiling over a flat plate including multimode film boiling [44]. Prior to this, Yang et al. [43] had used an adaptive CLSVOF method on triangular grids with an Eulerian-Lagrangian advection scheme, and studied its performance for advection cases and droplet deformation. Later Balcázar et al. [45] presented a coupled VOF/LS method applicable to 2D and 3D unstructured grids and assessed its performance for buoyant bubbles and a droplet in shear flow. In their method, the interface normals required for interface reconstruction are calculated using the least-squares gradient of discrete volume fraction distribution, while for curvature computation the normals are again determined from the least-squares gradient of the geometrically reinitialized distance function.

Another approach towards coupling LS and VOF methods is the VOSET method by Sun and Tao [46]. In this method, the LS advection equation is not solved and thus, it is highlighted to be simpler than CLSVOF method. However, in the numerical approach outlined for the VOSET method, it involves reconstruction of interface twice in a given time step; first using VOF PLIC algorithm and later using the distance function. Also the calculation of distance function is iterative requiring one to three iterations. Thus a comparison of the VOSET and CLSVOF methods in terms of computational expense by including these in a two-phase flow computational framework can be an interesting study, though beyond the scope of current work. The VOSET method was used by Guo et al. [47] to simulate two-dimensional horizontal film boiling. The method was extended to 3D by Ling et al. [48], and for two-dimensional triangular unstructured grid by Cao et al. [49] for two-phase problems without phase change.

Several algebraic approaches for implementing CLSVOF method have also been reported in the literature [50–53], usually using an algebraic compressive scheme for volume fraction advection.

Ferrari et al. [53] have recently presented a flexible CLSVOF method for non-uniform and unstructured grids, and performed numerical studies on some two-phase flows including bubbles in circular micro-channels. The algebraic methods have the limitation of a diffused interface resulting from the algebraic advection of the volume fraction. Tsui et al. [54] used a CLSVOF method for 2D static bubble and 3D single rising bubble problem on structured grids, using their modified VOF method [22] discussed earlier, while reinitializing the level set field algebraically. For the methods discussed in the above lines, a quantitative validation with advection test cases has not been presented.

From the aforementioned discussion, a few key observations emerge. The accurate modelling of interfacial phenomena is the prime concern for direct numerical simulation of two-phase flows. However, the computational cost sometimes outweighs the accuracy achieved by higher order interface reconstruction techniques. The PLIC scheme in the VOF methods is still the most widely used along with accurate surface tension modelling incorporated in the computational framework. The VOF method with height function curvature estimation as well as the CLSVOF methods present themselves as alternatives against higher order parabolic, spline or least squares interface reconstruction. For the CLSVOF method, researchers are employing different methodologies with respect to the VOF and LS calculations, as well as their coupling to improve the robustness, accuracy and computational efficacy of the method. Efforts are directed towards multi-directional advection to evolve it into a more practical method applicable to complex geometries with non-orthogonal or unstructured grids, which also reduces the computational cost. However, only a few studies exist for the CLSVOF method on unstructured grids [43,45,53] for some two-phase flow configurations. Moreover, none of these studies incorporate phase change modelling. Thus, it is imperative to establish a firm methodology in this direction, along with a detailed qualitative and quantitative validation using a number of advection as well as two-phase flow tests, so as to be able to study many more problems of practical interest in future.

The present study thus aims to build a CLSVOF method on unstructured grids for two-phase flows including phase change. We build upon the CLSVOF method proposed by Ningegowda and Premachandran [40] for non-uniform grids, and similarly use the accurate EMFPA VOF algorithm of López et al. [9], in conjunction with the LS method on unstructured quadrilateral and triangular grids. Further, within the EMFPA algorithm, we construct the flux polygons directly from the vertex velocities along with a scaling factor approach to correct the advected fluxes, to simplify this step in terms of computational complexity as well as cost. The performance of the present CLSVOF method is assessed through standard advection test cases, two-phase flow problems with surface tension followed by phase change modelling to simulate film boiling flows. For film boiling, results for saturated horizontal film boiling on a flat plate using structured and unstructured grids are presented first, before proceeding to simulate two-dimensional natural convection film boiling over a horizontal cylinder.

2. Mathematical formulation and numerical methodology

2.1. Governing equations for two-phase flows with and without phase change

In laminar regime for incompressible flow, considering a two-phase computational cell having a part of the interface, the continuity equation is given as [3,38,55]:

$$\int_{S_c} \mathbf{V} \cdot \mathbf{n} \, dS + \int_{S_{int}(t)} \|\mathbf{V} - \mathbf{V}_{int}\| \cdot \mathbf{n} \, dS = 0 \quad (1)$$

where S_c is the boundary of the computational cell, $S_{int}(t)$ is the interface between the two phases moving with a velocity \mathbf{V}_{int} , \mathbf{n} is the interface unit normal pointing into the liquid phase, and $\|\cdot\|$ represents the jump in the variable across the phase interface. The mass and energy jump conditions at the interface are given as:

$$\|\rho(\mathbf{V} - \mathbf{V}_{int})\| \cdot \mathbf{n} = 0 \quad (2)$$

$$\dot{m}h_{lv} = \|\mathbf{q}_{int}''\| \cdot \mathbf{n} \quad (3)$$

where \dot{m} is the mass flux across the phase interface, h_{lv} is the latent heat of vaporization and \mathbf{q}_{int}'' is the heat flux vector at the interface. Using the above jump conditions at the interface, the continuity equation is written as [3,38,55]:

$$\int_{S_c} \mathbf{V} \cdot \mathbf{n} dS + \int_{S_{int}(t)} \left(\frac{1}{\rho_l} - \frac{1}{\rho_v} \right) \frac{\|\mathbf{q}_{int}''\| \cdot \mathbf{n}}{h_{lv}} dS = 0 \quad (4)$$

Here the second term in Eq. (4) is non-zero only in two-phase cells for problems with phase change.

The momentum equation in the conservative form for the entire flow field is given as:

$$\frac{\partial(\rho\mathbf{V})}{\partial t} + \nabla \cdot (\rho\mathbf{V}\mathbf{V}) = -\nabla P + \nabla \cdot \boldsymbol{\tau} + \rho\mathbf{g} + \mathbf{F}_{st} \quad (5)$$

$\boldsymbol{\tau} = \mu(\nabla\mathbf{V} + \nabla\mathbf{V}^T)$ is the deviatoric stress tensor for a Newtonian fluid. \mathbf{F}_{st} represents the surface tension force acting only in the interface region and is included as a body force in the momentum equation following the continuum surface force (CSF) model of Brackbill et al. [56]. Neglecting any variations in the surface tension coefficient σ , the surface tension force per unit volume is given as $\mathbf{F}_{st} = \sigma\kappa\mathbf{n}\delta$ where δ is a delta function centered at the interface.

For two-phase flows with phase change, the energy equation needs to be solved to determine the temperature field within both the phases. However, for the cases of saturated film boiling considered in the present study, the liquid and the interface temperature is considered to be constant at the saturation temperature [3,23,30,38,55]. The energy equation is solved only in the vapor phase, and is given as:

$$\rho c_p \left(\frac{\partial T}{\partial t} + \mathbf{V} \cdot \nabla T \right) = \nabla \cdot (k\nabla T) \quad (6)$$

2.2. CLSVOF method: algorithm for interface reconstruction and advection

In the present CLSVOF method, once the velocity and temperature (for phase change problems) in the domain at an instant of time are determined, the volume fraction (F) and the level set (ϕ) fields are advected, and a piecewise linear interface in each cell is geometrically reconstructed. Further, the level set field is geometrically reinitialized with the reconstructed interface. The details of the above geometrical procedure are presented in the following subsections.

2.2.1. Volume of fluid advection

The volume fraction or the colour function F , is assigned a value of zero in the continuous phase, unity in the discrete phase and takes a value between zero and one in a two-phase cell. For interface capturing, one of the tasks is to advect the volume fraction F in space, at each time step, to get its value at the next time step. The equation governing the advection of F is given as:

$$\frac{\partial F}{\partial t} + \nabla \cdot (\mathbf{V}F) = F_{mt} \quad (7)$$

Here F_{mt} is the rate of generation of volume fraction due to mass transfer at the interface for phase change problems. For a

two-phase computational cell with volume as V_{cell} and having an interface with surface area S_{int}

$$F_{mt} = V_{mt} \left(\frac{S_{int}}{V_{cell}} \right) \quad (8)$$

where V_{mt} is the interfacial velocity due to mass transfer. For problems not involving phase change, the above term is zero.

The VOF advection equation (Eq. (7)) is solved in an unsplit manner using the Edge matched Flux Polygon Advection (EMFPA) algorithm of López et al. [9]. The EMFPA algorithm is an accurate VOF advection procedure in two-dimensions where flux polygons are created for each cell face. A truncated polygon arising out of the intersection of the flux polygon with the reconstructed interface determines the fluid advected through the cell face. The truncated polygon is calculated following the procedure of López and Hernández [57]. A summation of fluid volumes advected (positive for fluid leaving the cell and negative for fluid entering into the cell) through all the faces of a cell gives the total volume of fluid advected through that cell.

Fig. 1 shows the flux polygon along with the reconstructed interface in a computational cell. In the work of López et al. [9], the cell vertex velocities (at points 1 and 2) at intermediate time steps are used to determine the slopes of the edges of the flux polygons while the area of the flux polygon (A_d) is calculated using the face velocity (face 1–2). From this information, the location of points 3 and 4 (Fig. 1) can be determined using an iterative or a complex analytical procedure [57]. In order to simplify this step in terms of complexity as well as cost, a scaling factor based approach is used. In the present study, the flux polygon is directly constructed from the vertex velocities. If the area of the flux polygon constructed is A_p , the flux factor is given as $|A_d|/|A_p|$. The volume of fluid advected through the face is then the truncated polygon area corrected by this flux factor. Such a scaling approach is used by Liovic et al. [58] in their 3D unsplit VOF method, while López et al. [9] themselves prescribe such scaling for flux polygon construction in cases where the velocity is nearly parallel to the cell face and the CFL number is high. In the VOF framework of Jofre et al. [59], the fluxed volumes are also calculated based on cell vertex velocities. However, they used an analytical approach for volume reinforcement instead of a scaling approach used in the present study.

2.2.2. Level set advection

In the present CLSVOF method, the level set field is advected by solving the advection equation [30] given as:

$$\frac{\partial \phi}{\partial t} + (\mathbf{V}_{int} \cdot \nabla) \phi = 0 \quad (9)$$

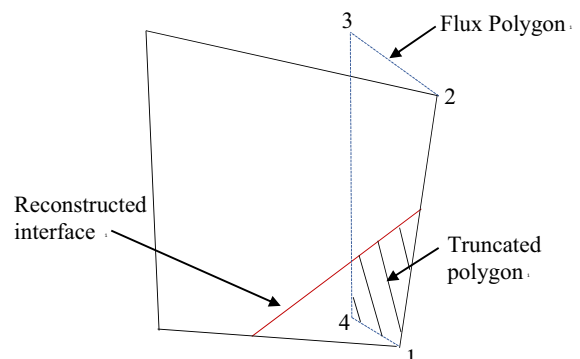


Fig. 1. A computational cell with the geometric entities involved in the unsplit EMFPA advection algorithm of López et al. [9].

where $\mathbf{V}_{int} = \mathbf{V} + \mathbf{V}_{mt}$, the sum of cell fluid velocity and interfacial velocity due to mass transfer. In the case of two-phase flows without phase change, the interface follows only the fluid velocity and $\mathbf{V}_{mt} = 0$. For solving the level set advection equation, a TVD scheme for unstructured grids proposed by Darwish and Moukalled [60] along with a Min-Max flux limiter function is used.

2.2.3. Geometrical interface reconstruction and level set reinitialization

A piecewise linear phase interface is geometrically reconstructed in each two-phase cell once the advected volume fraction and the level set fields are calculated. The interface normal is calculated from the level set field as:

$$\mathbf{n} = \frac{\nabla\phi}{|\nabla\phi|} \quad (10)$$

The gradient of the level set function is evaluated using a second-order accurate scheme based on a multi-dimensional Taylor series expansion proposed by Lehnhäuser and Schäfer [61] for unstructured grids. Knowing the interface normal and the colour function value in a two-phase cell, the exact location of the interface is evaluated using an analytical procedure for volume reinforcement given by López and Hernández [57].

In the CLSVOF method of Balcázar et al. [45], in the interface reconstruction step, the interface normal is calculated using a least squares gradient of the discrete volume fraction, and level set advection is not used. The interface normal is again calculated using a least squares gradient of the level set field during curvature calculation. The VOSET method by Sun and Tao [46] does not use level set advection but requires interface reconstruction step to be performed twice, which is computationally expensive for unstructured grids. The present CLSVOF method for unstructured grids adopts a more traditional approach [34,35] by calculating the interface normal only once using the advected level set field, as described above.

At the end of each time step, the level set field is geometrically reinitialized using the reconstructed piecewise linear geometric interface to maintain it to be a signed distance function. The geometric reinitialization procedure described by Son and Hur [35] is extended to unstructured grids in the present work. The distance function is computed only in a band of nearly four computational cells on either side of the interface.

2.2.4. Calculation of properties, surface tension and interfacial heat flux

In the present work, any fluid property χ (such as density, viscosity, thermal conductivity, specific heat) is calculated using a smoothed Heaviside function $H(\phi)$ as:

$$\chi = \chi_v + (\chi_l - \chi_v)H(\phi) \quad (11)$$

The smoothed Heaviside function prevents numerical instability arising due to discontinuous properties at the interface, and is given as [35]:

$$\begin{aligned} H(\phi) &= 0.5 + \frac{\phi}{2\varepsilon} + \frac{1}{2\pi} \sin\left(\frac{\pi\phi}{\varepsilon}\right) && \text{if } |\phi| \leq \varepsilon \\ &= 1 && \text{if } \phi > \varepsilon \\ &= 0 && \text{if } \phi < -\varepsilon \end{aligned} \quad (12)$$

The parameter ε controls the spread or the thickness of the interface for smoothing of properties and surface tension calculation. In the present study, it is taken as $1.5h$ for structured and unstructured quadrangular grids while $1.0h$ for triangular grids, where h is the characteristic grid size. For film boiling over a

cylinder presented later, the quadrilateral grid size is fine near the cylinder and very coarse in some parts of the domain. In such a case, h is replaced by the square root of the area of the cell.

As mentioned in Section 2.1, the surface tension is included as a volumetric source term in the momentum equation following the continuum surface force (CSF) model of Brackbill et al. [56] and is given as $F_{st} = \sigma\kappa\mathbf{n}\delta$ where δ is a delta function centered at the interface. In the present CLSVOF method, $\mathbf{n}\delta$ is calculated as the gradient of the Heaviside function [35]. The surface tension force is then calculated as:

$$F_{st} = \sigma\kappa\nabla H \quad (13)$$

The curvature is calculated as:

$$\kappa = -\nabla \cdot \left(\frac{\nabla\phi}{|\nabla\phi|} \right) \quad (14)$$

In calculating the curvature and the gradient of Heaviside function, the multi-dimensional Taylor series expansion proposed by Lehnhäuser and Schäfer [61] for unstructured grids is used.

For phase change problems, in order to determine the interfacial mass flux using the energy jump condition specified in Eq. (3), the heat flux at the interface needs to be calculated. At the phase interface, the heat flux is calculated as

$$\|\mathbf{q}_{int}''\| \cdot \mathbf{n} = k_v \left(\frac{T_v - T_{int}}{\Delta n} \right) - k_l \left(\frac{T_{int} - T_l}{\Delta n} \right) \quad (15)$$

where T_v and T_l are the temperatures of the vapor and liquid phases at a normal distance Δn from the interface. In the present study, saturated film boiling is studied and thus, the heat flux needs to be calculated only in the vapor phase. The mid-point of the interface segment in the two-phase cell is taken to be at the saturation temperature. From the reconstructed interface geometry, and the temperature distribution in the cells surrounding the interface cell obtained by solving the energy equation in the vapor phase, the vapor side heat flux is calculated [3]. Further, knowing the interfacial heat flux, the temperature in the two-phase cells is extrapolated from the interface.

2.3. Two-phase solver

In the present work, a two-phase flow solver for unstructured collocated grids is developed based on the unstructured finite volume method of Sun et al. [62]. The convective terms in the momentum and energy equations are discretized using a second order upwind scheme for unstructured grids. The SIMPLE algorithm [63] is used for pressure and velocity coupling. The time integration is performed using a first order Euler explicit scheme. The time step size is selected after consideration of various time step constraints, based on grid size h , as given below.

$$\Delta t < \min \left(\frac{h}{\|\mathbf{V}\|}, \left(\frac{h}{\|\mathbf{g}\|} \right)^{0.5}, \frac{\rho h^2}{\mu}, \left(\frac{(\rho_1 + \rho_2)h^3}{4\pi\sigma} \right)^{0.5} \right) \quad (16)$$

The first three terms denote time step constraints imposed due to CFL condition, gravity and viscous effects. The last term governs the stability condition for the explicit treatment of the surface tension force, given by Brackbill et al. [56].

3. Results and discussion

In the following subsections, the performance of the present CLSVOF method is assessed. In most of the earlier studies on unstructured grids discussed in the introduction section, using the CLSVOF as well as other methods, a detailed quantitative validation of the method with both advection and two-phase flow

tests has not been carried out. In the present study, a detailed qualitative as well as quantitative validation of results are presented for various advection test cases, and two-phase problems with and without phase change, for both structured and unstructured grids. First, several advection test cases, which help to estimate the accuracy of interface reconstruction and advection, are considered. Then problems, in which the CLSVOF method is coupled to the two-phase flow solver and interfacial tension is accounted for, are studied. Finally, phase change model is incorporated and results for boiling are presented.

3.1. Benchmark advection test problems

In these test cases, the velocity field in the domain is analytically specified. Hence, these tests help to assess the performance of the interface advection and reconstruction algorithm. The CFL number is calculated based on the maximum velocity in the domain as $|U_{max}| \Delta t / h$, where h is the characteristic size of the grid elements. For the case of unstructured grids, the length scale for calculating the CFL number is considered to be the same as for the corresponding structured grid. This poses an additional stringency on unstructured grids based on the CFL number, since the distance between two grid points may be less than h at different locations in the grid. However, in all the simulations, the CFL number at any point in the domain is less than 1.

Apart from the qualitative information obtained from interface shape and location, the values of L_1 and L_2 error norms obtained from the present CLSVOF method are compared with those available in literature to quantify the performance of the present method. These are defined as [9]:

$$L_1 = \sum_{i=1}^N |F_i^{calculated} - F_i^{exact}| A_i \quad (17)$$

$$L_2 = \frac{\sum_{i=1}^N |F_i^{calculated} - F_i^{exact}|}{\sum_{i=1}^N F_i^{exact}} \quad (18)$$

Here F_i and A_i are respectively the volume fraction and area of the i^{th} cell.

3.1.1. Simple translation of a circle

One of the preliminary tests to assess the accuracy of interface reconstruction and advection is the translation of a circular fluid body. A circle of fluid of radius 0.2 units is initially placed at (0.25, 0.25) in a square domain of 1×1 . It is advected by a velocity field $u = 1$, $v = 1$ for a time $t = 0.5$ units. A grid size of $h = 1/40$ is considered. The resulting L_1 error norms are plotted as a function

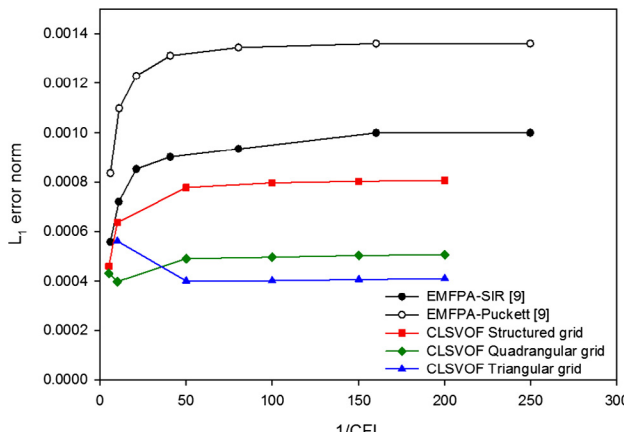


Fig. 2. L_1 error norm variation with CFL number for grid size = $1/40$.

of CFL number in Fig. 2 and compared with the results of López et al. [9], where they proposed a VOF method with EMFPA advection and a higher order spline based interface reconstruction instead of the PLIC algorithm. Additionally, for this test case, they also presented results using Puckett's iterative interface reconstruction method [64]. Since EMFPA algorithm is employed for advection of VOF function in the present CLSVOF method also, the lower levels of error norms for different grid geometries particularly depict the accuracy of interface reconstruction with the coupling of the level set and the VOF PLIC methods. Lower error with unstructured grids can be attributed to an extent on the relatively higher number of cells for the same characteristic grid size. Similar to the compared results, the L_1 error remains bounded as the CFL number decreases. However, for unstructured quadrangular and triangular grids, beyond some point, the errors tend to increase for higher values of CFL number. This signifies the need for a careful choice of a reasonably low value of CFL number for subsequent two-phase flow simulations, as done in the CLSVOF method proposed by Balcázar et al. [45] as well as the VOSET method by Cao et al. [49].

In Fig. 3, the normalized L_1 error norms with different grid geometry and size are compared with the results of Tsui and Lin [22] for a CFL number of 0.1. The normalized L_1 norms are calculated as:

$$\text{Normalized } L_1 = \frac{\sum_{i=1}^N |F_i^{calculated} - F_i^{exact}| A_i}{\sum_{i=1}^N F_i^{initial} A_i} \quad (19)$$

Tsui and Lin [22] proposed a VOF method (CISIT scheme) for two-phase flows on structured as well as unstructured grids. Later, Tsui et al. [23] extended the CISIT method to simulate film boiling. Hence the comparison in Fig. 3 is presented to evaluate the present CLSVOF method, which is also eventually used to simulate film boiling. For the test case of simple translation of a circle, however, quantitative results are available only for structured grids with CISIT method. As can be seen in Fig. 3, the normalized L_1 error norms obtained with the present CLSVOF method are an order of magnitude lower than the VOF based CISIT method, again showing the accuracy of the present method.

3.1.2. Zalesak slotted disk rotation

This test case proposed by Zalesak [65] is widely used in literature for assessing interface tracking or capturing algorithms. In this test case, the rotation of a slotted circular disk placed in a square domain with uniform vorticity field is considered. For the sake of

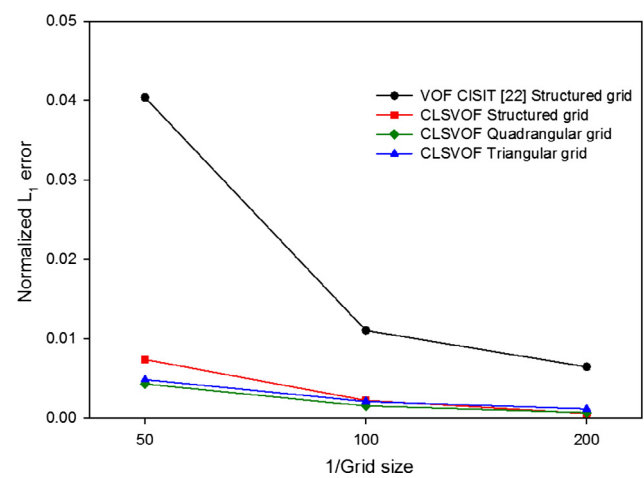


Fig. 3. Normalized L_1 error for translation of a circle with different grid geometry and size at CFL = 0.1.

comparison, the geometry and conditions corresponding to the work of Rudman [66] are used in the present study. These parameters have also been used by López et al. [9] and Yang et al. [43]. The domain size is 4×4 in which a disc of radius 0.15 is centered at (2, 2.75). The slot width and height are 0.12 and 0.6, respectively. A grid size of $h = 1/50$ corresponding to 200 rectangular cells in each coordinate direction is considered. The velocity components are given as:

$$u = \frac{\pi}{6.31} (2.0 - y) \quad \text{and} \quad v = \frac{\pi}{6.31} (x - 2.0) \quad (20)$$

In this test case, the CFL number based on maximum velocity in the domain is 0.25. The disc returns to its original position after 2524 time steps. The shape of the disc after one complete rotation obtained with structured, unstructured quadrangular, and unstructured triangular grids is shown in Fig. 4. The smoothing of the sharp corners as well as a slight distortion of the interface near them is observed. The smoothing of the corners can be attributed to linear interface reconstruction in each cell. With the triangular mesh, the final shape is more symmetric and less distorted similar to the one obtained by Yang et al. [43] with adaptive triangular grid. On the structured as well as the unstructured quadrangular grids, the final interface shape obtained by the present CLSVOF method with linear interface reconstruction is similar to that observed by López et al. [9] with spline interface reconstruction on structured grid.

To further assess the results, L_2 error norms are presented in Table 1. The magnitude of the error norms with structured and unstructured quadrangular grids is comparable to some of the higher order interface reconstruction methods assessed by López et al. [9], such as spline interface reconstruction, Puckett's iterative method, and the least-square fit based interface reconstruction. For an unstructured mesh with triangular cells, the error is lower than the adaptive CLSVOF method of Yang et al. [43]. These observations with the present CLSVOF method are important since the extension of most of the higher order methods to problems such as boiling for unstructured grids may be deterred by the fact that these are reported to be computationally intensive. The present method thus provides a more practical approach with good accuracy. This test case was also used by Cao et al. [49] to validate the VOSET method for unstructured grids, but only qualitative results are available for the same.

3.1.3. Time-reversed single vortex flow test

In this test case, a circle of fluid is advected by a single vortex flow field leading to spiralling of the fluid structure towards the vortex center together with large topological changes. In the time-reversed test used by Rider and Kothe [19], the flow changes direction after half time period of the flow and the fluid returns to its original location at the final instant of the time period. We consider the test case with time period $T = 8$ s, which leads to a large

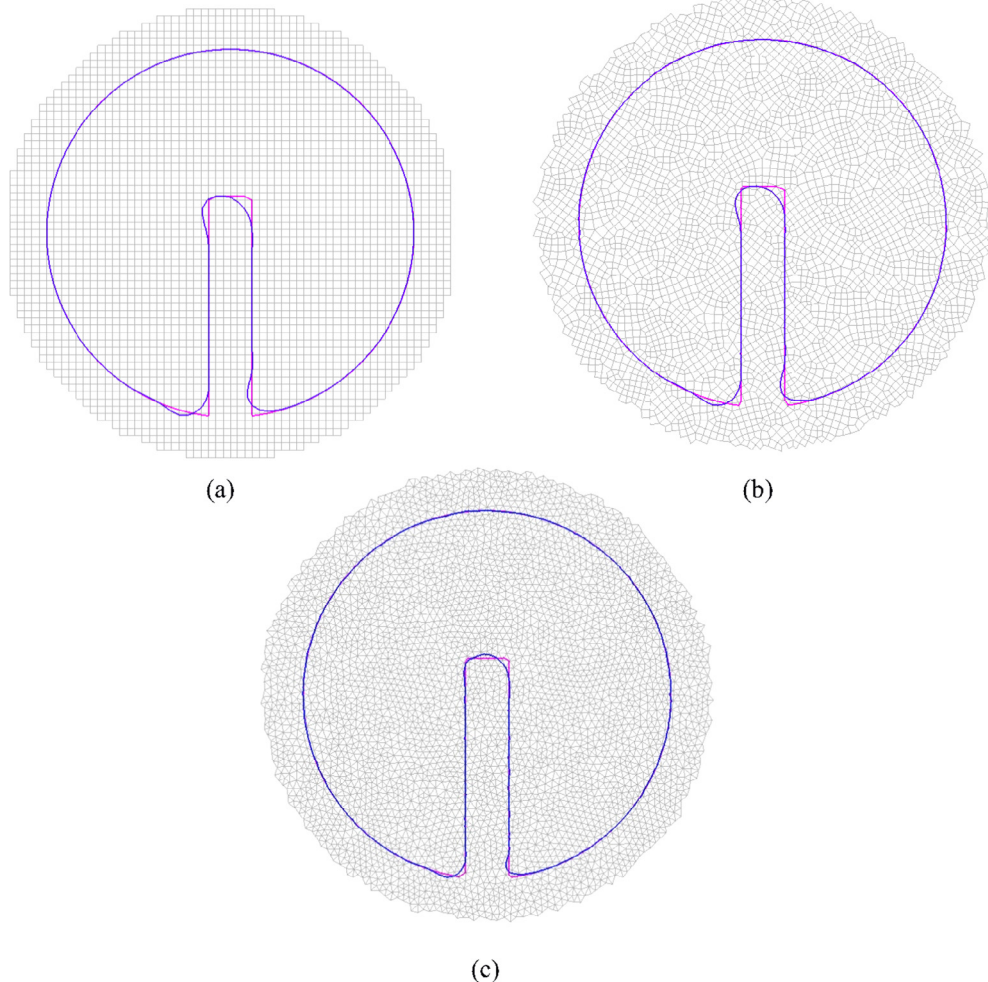


Fig. 4. Interface shape after one complete revolution of Zalesak slotted disk (a) structured grid (b) quadrangular grid (c) triangular grid (pink: initial shape, blue: final shape). (For interpretation of the references to color in this figure legend, the reader is referred to the web version of this article.)

Table 1 L_2 error norms for rotation of Zalesak slotted disc.

| Advection/reconstruction algorithm | L_2 error norm |
|------------------------------------------------------|-----------------------|
| <i>Structured Grid</i> | |
| Youngs | 1.09×10^{-2} |
| EMFPA/Youngs | 1.06×10^{-2} |
| EMFPA/Puckett | 9.73×10^{-3} |
| EMFPA/SIR | 8.74×10^{-3} |
| Scardovelli and Zaleski (linear least-square fit) | 9.42×10^{-3} |
| Scardovelli and Zaleski (quadratic fit) | 5.47×10^{-3} |
| Scardovelli and Zaleski (quadratic fit + continuity) | 4.16×10^{-3} |
| Present CLSVOF method | 9.82×10^{-3} |
| <i>Unstructured Grid</i> | |
| ACLSVOF (uniform triangular grid) [43] | 7.19×10^{-3} |
| ACLSVOF (adaptive triangular grid) [43] | 1.25×10^{-2} |
| Present CLSVOF method (quadrangular grid) | 1.04×10^{-2} |
| Present CLSVOF method (triangular grid) | 5.20×10^{-3} |

Results other than those from [43] are taken from Table 3 of López et al. [9].

interface deformation. The circular fluid body of radius 0.15 is placed at (0.5, 0.75) in a domain of 1×1 . The grid size is $h = 1/128$. The velocity field is specified as:

$$u = -\sin(2\pi y) \sin^2(\pi x) \cos(\pi t/T) \quad \text{and} \\ v = \sin(2\pi x) \sin^2(\pi y) \cos(\pi t/T) \quad (21)$$

Fig. 5 shows the interface shapes obtained after half and final instant of the time period with different mesh types. As the fluid element spirals towards the vortex center, its thickness continues to decrease leading to breakup starting from the tail, primarily on account of grid resolution. Qualitatively, the results obtained with the present CLSVOF method on structured and unstructured quadrangular grid, shown in Fig. 5(a) and (b) respectively, at time instants $t = T/2$ and $t = T$ are quite similar to those achieved with EMFPA advection and Youngs' PLIC interface reconstruction by López et al. [9] for structured grid. With other higher order interface reconstruction methods used in [9], the filament breakup is less or completely avoided. From Fig. 5(c) it can be seen that with the unstructured triangular grid, a similar shape is obtained at time $t = T/2$ as with the other grid geometries. At time $t = T$, the shape is quite close to the original circle except at the top where a very small segment is separated from the main fluid structure, which is plausible due to the use of a completely unstructured triangular grid. In Fig. 5(d), the interface shape obtained by Balcázar et al. [67] using a conservative level set method proposed for unstructured grids is shown. In their study, a grid with 2.1×10^5 cells is used. The results with the present CLSVOF method (4.3×10^4 triangles) are closer to the original interface shape at the final time instant. Cao et al. [49] have carried out the single vortex flow test case with the VOSET method on triangular grid and also shown the qualitative interface shape to be better than the level set method [67] with a coarser mesh.

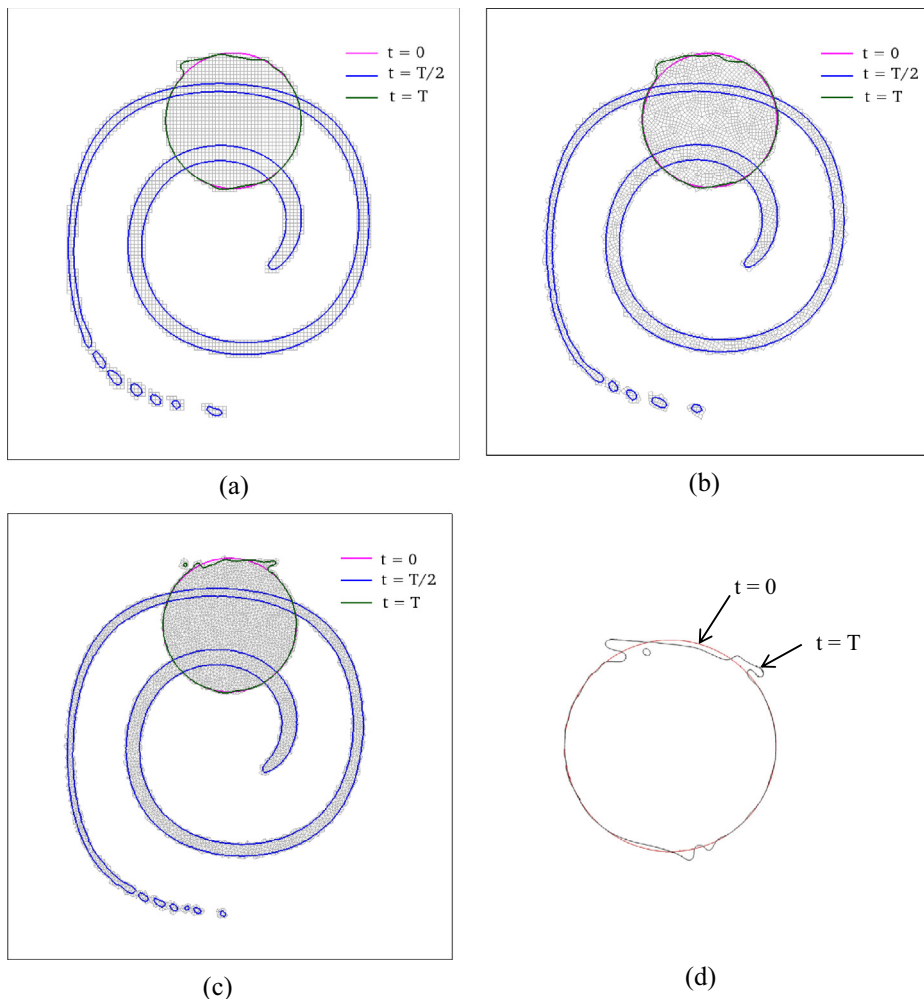


Fig. 5. Results for time-reversed single vortex flow ($T = 8$ s) (a) structured grid (b) quadrangular grid (c) triangular grid (d) conservative level set method, Balcázar et al. [67].

In Table 2, the values of L_1 error norms are presented for the quantitative assessment of present results. A comparison of error norms with different advection and interface reconstruction methods presented by López et al. [9] on structured grids, is also included in Table 2. For unstructured grids, quantitative results are available for the adaptive CLSVOF method by Yang et al. [43] on triangular grids. With the present method, the error is highest with the unstructured quadrangular grid. From the structured grid results, it can be seen that with the present CLSVOF method the error is lower than Youngs interface reconstruction, while it is slightly higher when compared to spline or Puckett's iterative interface reconstruction. For triangular grid, errors obtained with the adaptive CLSVOF method by Yang et al. [43] are lower. Overall, the magnitude of error norms obtained with the present CLSVOF method is comparable for structured and unstructured grids, and is not substantially higher than other methods discussed above. The qualitative and quantitative results from this test case depict the ability of the present CLSVOF method to handle large topological changes with good accuracy.

3.2. Two-phase flow solver with interfacial tension

After assessing the performance of interface advection and reconstruction, the interface capturing algorithm is coupled with the flow solver and the surface tension effect is included. Static liquid drop, Rayleigh-Taylor instability and rising gas bubble problems are considered to evaluate the two-phase flow solver with the present CLSVOF method on unstructured grids.

3.2.1. Static liquid drop

For a static liquid drop in equilibrium, any numerical algorithm used to model interfacial tension should lead to a balance of surface tension force with the pressure jump condition at the interface, given by Young-Laplace law as

$$\Delta P_{\text{exact}} = \sigma \kappa_{\text{exact}} \quad (22)$$

The exact curvature for a circular drop of radius R is given by $\kappa_{\text{exact}} = 1/R$. Moreover, in the absence of any other forces, the velocity in the domain should ideally be zero. The Continuum Surface Force (CSF) method of Brackbill et al. [56] has been widely used for modelling surface tension force with the VOF as well as the level set based methods. It allows the interfacial force to be considered as a volume force that is included as a source term in the discretized Navier-Stokes equations. However, the CSF method produces unphysical spurious currents due to inaccurate curvature estimation with discrete volume fraction distribution that usually appear as vortex-like structures in the vicinity of the interface. As discussed earlier in the introduction section, various methods

and techniques were proposed in the literature on the reduction of these spurious currents by accurate curvature estimation and exact balance of pressure gradient with surface tension force. In the CLSVOF method, accurate curvature is estimated by calculating the gradients of a smooth level set function instead of a discontinuous colour function used in the VOF methods.

The characterization of spurious currents and pressure jump solution with the present CLSVOF method is done by considering a static circular drop in equilibrium. The conditions used in the present study correspond to those used by Dupont and Legendre [68], who used a VOF method with successive filtering and smoothing of the colour function. With the VOF methods, the smoothing of the colour function gives improved results in the CSF framework [8]. Same conditions were earlier used by Renardy and Renardy [8] for evaluation of their parabolic reconstruction of surface tension (PROST) method, which has been shown to achieve a substantial reduction in spurious current levels as compared to the CSF formulation. In this problem, the drop of radius $R = 0.125$ is centered in a square domain of size 1×1 . Both the fluids have density of 4 and viscosity of 1, while the surface tension coefficient is 0.357. The corresponding Ohnesorge number ($\mu/(\sigma \rho R)^{0.5}$) for the case is 2.37. The cell size used is $1/96 (=R/12)$, while the time step used is $\Delta t = 10^{-5}$. The initial velocity and pressure fields are prescribed as zero in the domain. Results are presented after 20,000 time steps as in [68].

Fig. 6(a)–(c) shows the pressure distribution obtained in the domain with different grid types, while Fig. 6(d) shows the pressure normalized with ΔP_{exact} vs x/R at $y = 0.5$. These results show that the present method computes the pressure distribution as per Young-Laplace law for structured as well as unstructured grids. It is also observed that in all the cases, the drop center remains at the original position and its shape remains circular. In order to further assess the accuracy of the results, the L_1 norm for spurious velocities and the relative errors in pressure jump condition are calculated as given by Dupont and Legendre [68]:

$$L_1 = \frac{1}{N_{\text{cells}}} \sum_i^{N_{\text{cells}}} V_i \quad (23)$$

$$E_{\text{total}, \Delta P} = \frac{|\Delta P_{\text{total}} - \Delta P_{\text{exact}}|}{\Delta P_{\text{exact}}} \quad (24)$$

$$E_{o, \Delta P} = \frac{|\Delta P_o - \Delta P_{\text{exact}}|}{\Delta P_{\text{exact}}} \quad (25)$$

Here, ΔP_o is the difference in pressure at the drop center and the minimum pressure at the domain boundary. ΔP_{total} is the difference in averaged pressure inside and outside the drop, which includes the pressure values across the interface.

In Table 3, the L_1 norms for spurious velocities and relative errors in pressure jump condition obtained with structured and unstructured grids are compared with the results of Dupont and Legendre [68] on structured grid. It is observed that with the present method, the spurious currents are lowered in case of structured and triangular grids, while being slightly higher for quadrangular grid. It must also be noted that the comparison is done with the optimum results presented by Dupont and Legendre [68] obtained after a number of filtering and smoothing steps, without which the present results compare much better. The lower values of relative errors in pressure also indicate that the present method fulfills the Young-Laplace condition for all grid geometries with good accuracy.

3.2.2. Rayleigh-Taylor instability

A heavier fluid placed on top of a lighter fluid moves under the effect of gravity, in the presence of an initial perturbation. We

Table 2

L_1 error norms for single vortex flow test case.

| Advection/reconstruction algorithm | L_1 error norm |
|-------------------------------------------|-----------------------|
| <i>Structured Grid</i> | |
| Rider and Kothe/Puckett | 1.44×10^{-3} |
| Harvie and Fletcher/Youngs | 2.16×10^{-3} |
| Harvie and Fletcher/Puckett | 1.18×10^{-3} |
| EMFPA/Youngs | 2.13×10^{-3} |
| EMFPA/Puckett | 1.17×10^{-3} |
| EMFPA/SIR | 7.57×10^{-4} |
| Present CLSVOF method | 1.93×10^{-3} |
| <i>Unstructured Grid</i> | |
| ACLSVOF (uniform triangular grid) [43] | 5.61×10^{-4} |
| ACLSVOF (adaptive triangular grid) [43] | 5.09×10^{-4} |
| Present CLSVOF method (quadrangular grid) | 2.89×10^{-3} |
| Present CLSVOF method (triangular grid) | 1.85×10^{-3} |

Results other than those from [43] are taken from Table 7 of López et al. [9].

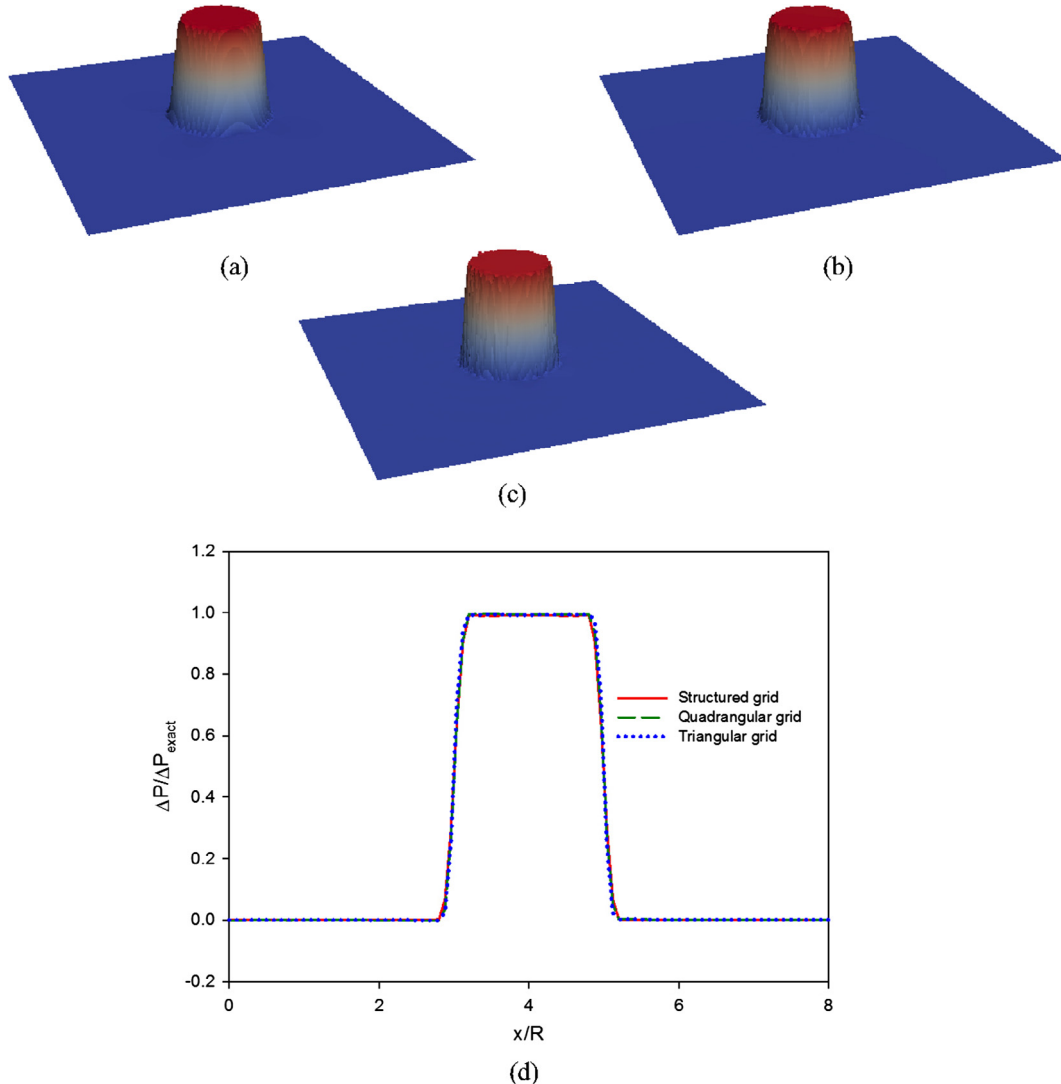


Fig. 6. Pressure distribution in the domain showing pressure jump across the interface (a) structured grid (b) quadrangular grid (c) triangular grid and (d) pressure normalized with ΔP_{exact} vs x/R at $y = 0.5$ for different mesh geometries.

Table 3
Errors in velocity and pressure jump for static circular drop with grid size $R/12$.

| | L_1 | $E_{\text{total},\Delta P}$ (%) | $E_{o,\Delta P}$ (%) |
|--------------------------|------------------------|---------------------------------|----------------------|
| Dupont and Legendre [68] | 8.326×10^{-5} | 6.6 | 0.6 |
| Structured grid | 2.241×10^{-5} | 5.84 | 0.76 |
| Quadrangular grid | 1.199×10^{-4} | 5.84 | 0.27 |
| Triangular grid | 7.802×10^{-5} | 4.86 | 0.47 |

consider the case where the effect of gravity exceeds the stabilizing effect of surface tension resulting in a large amplitude, and the growth of instability cannot be approximated by linear theory. The initial setup of the problem is shown in Fig. 7. The initial sinusoidal disturbance is defined based on an amplitude of 0.05 m. The problem has been studied by several researchers [69–71] for the validation of their numerical algorithm. The density of the heavier fluid is 1.225 kg/m^3 , while that of the lighter fluid is 0.1694 kg/m^3 . The viscosity of the two immiscible fluids is considered to be same as 0.00313 kg/ms , and the surface tension coefficient is 0.001337 N/m . The grid size used for the present simulation is $h = 1/128$. The corresponding number of cells for structured, quadrangular and triangular grids is 65,536, 84,103 and 174,248, respectively.

From Fig. 8, it can be seen that with the present CLSVOF method on structured as well as unstructured grids, an inverted mushroom shape is obtained with thin filaments appearing after 0.8 s. Popinet and Zaleski [69] have presented the results for this test case using a Lagrangian front tracking method, as well as a PLIC based method. They also showed the formation of thin filaments from an inverted mushroom shape beyond time $t = 0.8$ s. These thin filaments subsequently get fragmented due to inadequate grid resolution. However, they depicted that the front tracking algorithm could capture these thin structures even on a relatively coarse mesh (64×256) accurately. Zuzio and Estivalezes [70] studied the problem using a level set based ghost fluid method on an adaptive mesh. By increasing the grid resolution equivalent to 128×512 cells, they showed the filaments up to 0.9 s. With a modified VOF method to capture thin fluid structures within a single cell, López et al. [71] could capture the filaments without breaking up to 0.95 s.

From Fig. 8, it can be seen that the results for the present computation on different mesh types in terms of interface shape as well as location qualitatively agree quite well to all the aforementioned studies. The location of the lowermost point of the mushroom shape as well as interface regions near the wall matches very well with the results presented in [71], showing the accuracy

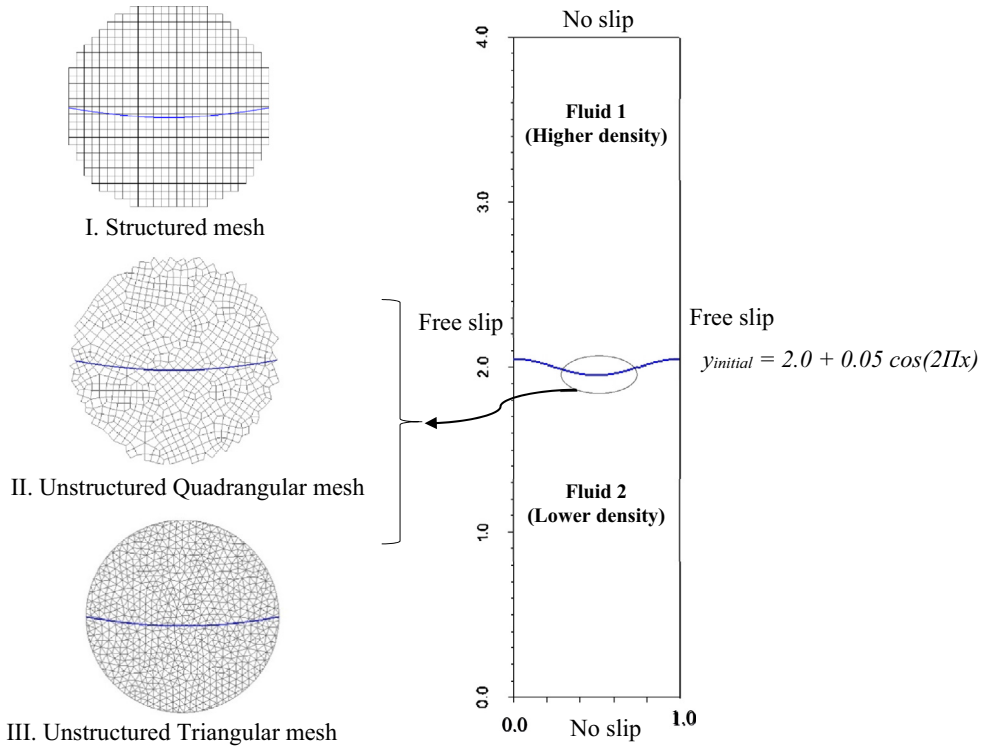


Fig. 7. Setup for Rayleigh-Taylor instability.

of the overall flow solution. With structured and quadrangular grids, a slight breakup of the thin filaments is observed at 0.9 s. However, it is not into the form of droplets as with the PLIC based method [69] shown in Fig. 8(d). The triangular grid having a greater number of cells for the same characteristic grid size, is able to capture the thin filaments without breakup similar to the results obtained by Zuzio and Estivalezes [70] on an adaptive grid as shown in Fig. 8(c), and results of Popinet and Zaleski [69] obtained with a front tracking algorithm shown in Fig. 8(d).

3.2.3. Rising gas bubble

A gas bubble placed in a column of a heavier fluid rises under the effect of gravity and deforms simultaneously. In the present study, the case studied by Hysing et al. [72] is considered. They have presented quantitative benchmark quantities in terms of bubble rise velocity, circularity and center of mass.

A bubble of diameter $d = 0.5$ units is placed at $(0.5, 0.5)$ in a domain with dimensions 1×2 as shown in Fig. 9. Ω_1 and Ω_2 represent the regions occupied by the heavier fluid and the gas bubble respectively. No slip boundary condition is specified at the horizontal walls, while slip condition is specified at the vertical walls. The velocity field is initialized as zero in the entire domain, and the pressure field is initialized as per hydrostatic theory. A constant pressure is specified inside the bubble initially. A mesh resolution of $h = 1/80$ ($=d/40$) is found suitable and used in the present study. The parameters for the simulation are given in Table 4. The Reynolds number and the Eötvös number are defined as:

$$Re = \frac{\rho_1 U d}{\mu_1} \quad (26)$$

$$Eo = \frac{\rho_1 U^2 d}{\sigma} \quad (27)$$

where $U = \sqrt{gd}$. In the present study, $Re = 35$ and $Eo = 10$ have been considered. Under these conditions, the surface tension effect is

substantial which does not allow any breakup, and finally the bubble ends up in an ellipsoidal regime [72].

In Fig. 10, the bubble shapes at different instants of time, obtained with structured, unstructured quadrangular and unstructured triangular grids are shown. With all the meshes, the results are identical. The final bubble shape matches well with that shown by Hysing et al. [72]. At time $t = 1$, the bubble is deformed at the base from the initially circular shape. Subsequently the bubble is stretched horizontally as shown at $t = 2$, and finally it attains a stable ellipsoidal shape.

For quantitative assessment of the results, the bubble rise velocity (v_c), circularity (ψ), and the center of mass (y_c) are calculated as given below:

$$v_c = \frac{\int_{\Omega_2} v dV}{\int_{\Omega_2} dV} \quad (28)$$

$$y_c = \frac{\int_{\Omega_2} y dV}{\int_{\Omega_2} dV} \quad (29)$$

$$\psi = \frac{\pi d}{P} \quad (30)$$

Here v is the vertical velocity component, y is the coordinate value in y -direction, and P represents the perimeter of the bubble.

The time evolution of above quantities is shown in Fig. 11. Results obtained with structured as well as unstructured grids compare well with those of Hysing et al. [72]. The rise velocity attains a maximum around 0.9 time units before the terminal velocity is achieved. The bubble circularity decreases as the bubble is stretched. An inflection in the curve is observed at nearly 1.9 time units after which the circularity increases owing to the surface tension restoring the bubble shape to a stable ellipsoid. The center of mass of the bubble varies almost linearly and is well captured with structured and unstructured grids.

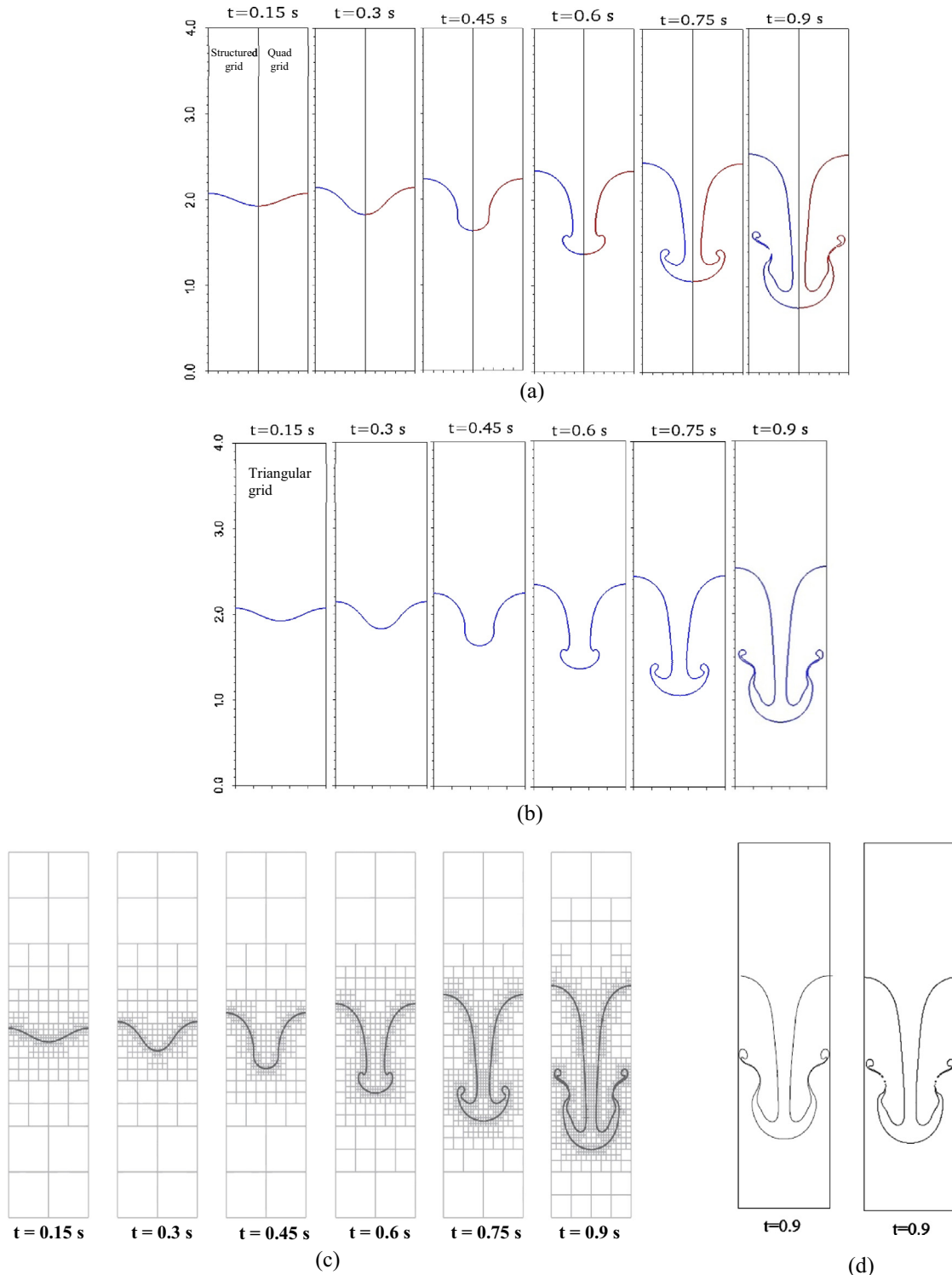


Fig. 8. Growth of Rayleigh-Taylor instability: Interface evolution (a) structured (I, left) and unstructured quadrangular (II, right) grid (b) triangular grid (III) (c) Zuzio and Estivalezes [70] (d) Popinet and Zaleski [69]. Front tracking method (left) and PLIC based method (right).

3.3. Film boiling

In the unstructured two-phase flow solver, the phase change model is incorporated and results for film boiling problems are presented. Saturated film boiling over a horizontal flat plate and a horizontal cylinder are considered for phase change problems. For film boiling over a flat plate, comparison of the present results with those available in the literature leads to the validation of the phase change model. Results for film boiling on a horizontal cylinder

present the ability of the present method to simulate phase change problems on complex geometries and fulfills our primary objective.

3.3.1. Film boiling over a horizontal flat plate

Saturated film boiling over a horizontal flat plate has been studied by several researchers numerically [1–3,23,28,30,38,73–75], and serves as an important problem to validate the phase change model incorporated in the present CLSVOF method. Water at near

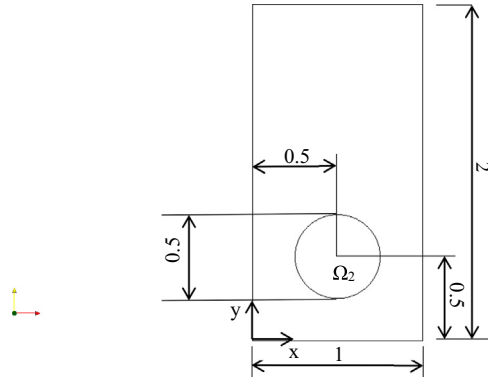


Fig. 9. Computational domain for the rising gas bubble problem with initial position of the bubble.

Table 4
Parameters considered for the rising gas bubble problem.

| ρ_1 | ρ_2 | μ_1 | μ_2 | g | σ |
|----------|----------|---------|---------|------|----------|
| 1000 | 100 | 10 | 1 | 0.98 | 24.5 |

critical conditions (21.9 MPa, 646 K) is considered in the present study. The corresponding properties of the liquid and vapor phases adopted from Tomar et al. [38] are given in Table 5. The characteristic capillary length scale for the problem is given as:

$$\lambda_o = \sqrt{\frac{\sigma}{(\rho_l - \rho_v)g}} \quad (31)$$

Previous studies have shown alternate bubble formation and departure at sites separated by a distance of $\lambda_d/2$, where λ_d is the most dangerous Taylor wavelength [76] and is given as $\lambda_d = 2\pi\sqrt{3}\lambda_o$. A domain of size $\lambda_d/2 \times \lambda_d$ is considered here due to the symmetry of the problem. At the top boundary, outflow boundary condition is used. No slip boundary condition is specified at the bottom boundary of the domain, while symmetry boundary condition is used at the left and right boundaries. The temperature at the bottom wall is specified as $T_w = T_{sat} + \Delta T$, where ΔT is the wall superheat and T_{sat} is the saturation temperature of water. In the present study, results are presented with a wall superheat of 5 K. A vapor film blankets the bottom superheated wall from the saturated liquid and the film thickness is initialized as:

$$\lambda = \frac{\lambda_d}{64} \left(2.0 + \cos\left(\frac{2\pi x}{\lambda_d}\right) \right) \quad (32)$$

This leads to maximum initial film thickness at the right boundary, $x = 0$ (node). The minimum initial film thickness is at the left boundary, $x = -\lambda_d/2$ (antinode). The initial velocity field in the domain is specified as zero. For the temperature, a linear variation from the wall temperature to the saturated liquid temperature is initialized in the vapor phase.

In addition to capturing the bubble release pattern, heat transfer results are quantitatively determined. The local Nusselt number (Nu) and the space-averaged Nusselt number \overline{Nu}_L at the heated wall are given as:

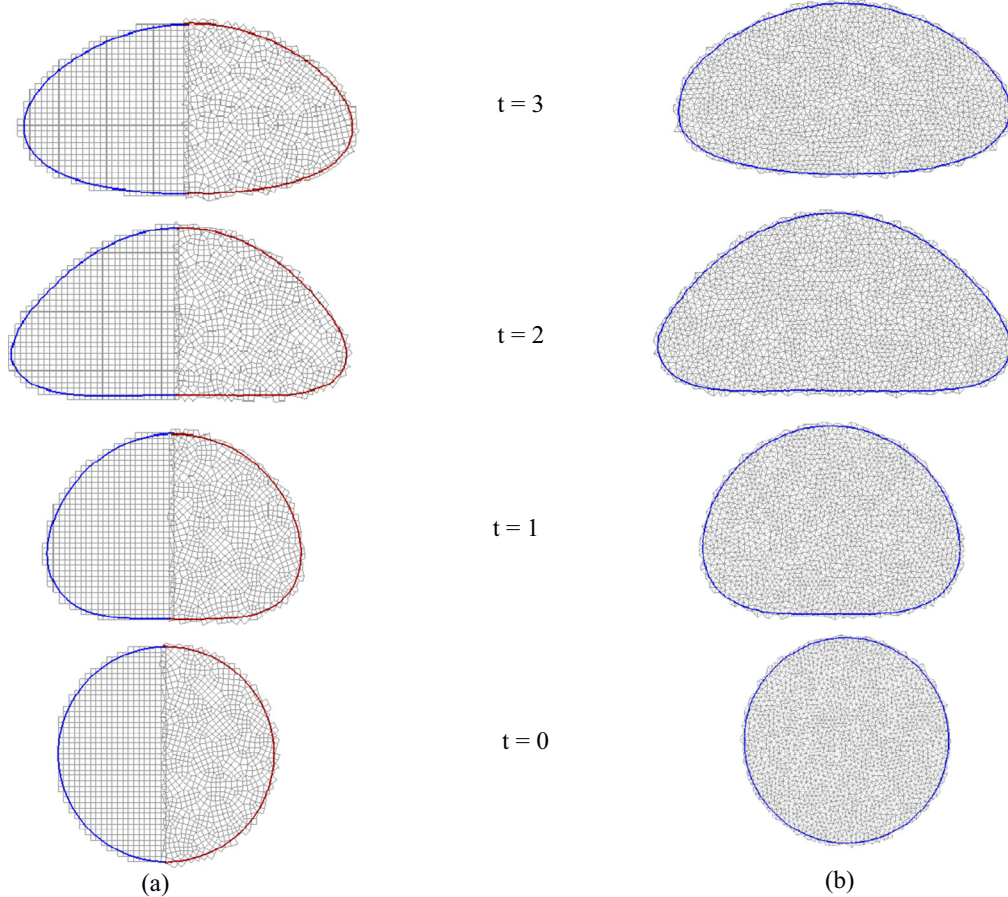


Fig. 10. Bubble shape at different time instants (a) structured grid (left); quadrangular grid (right) (b) triangular grid.

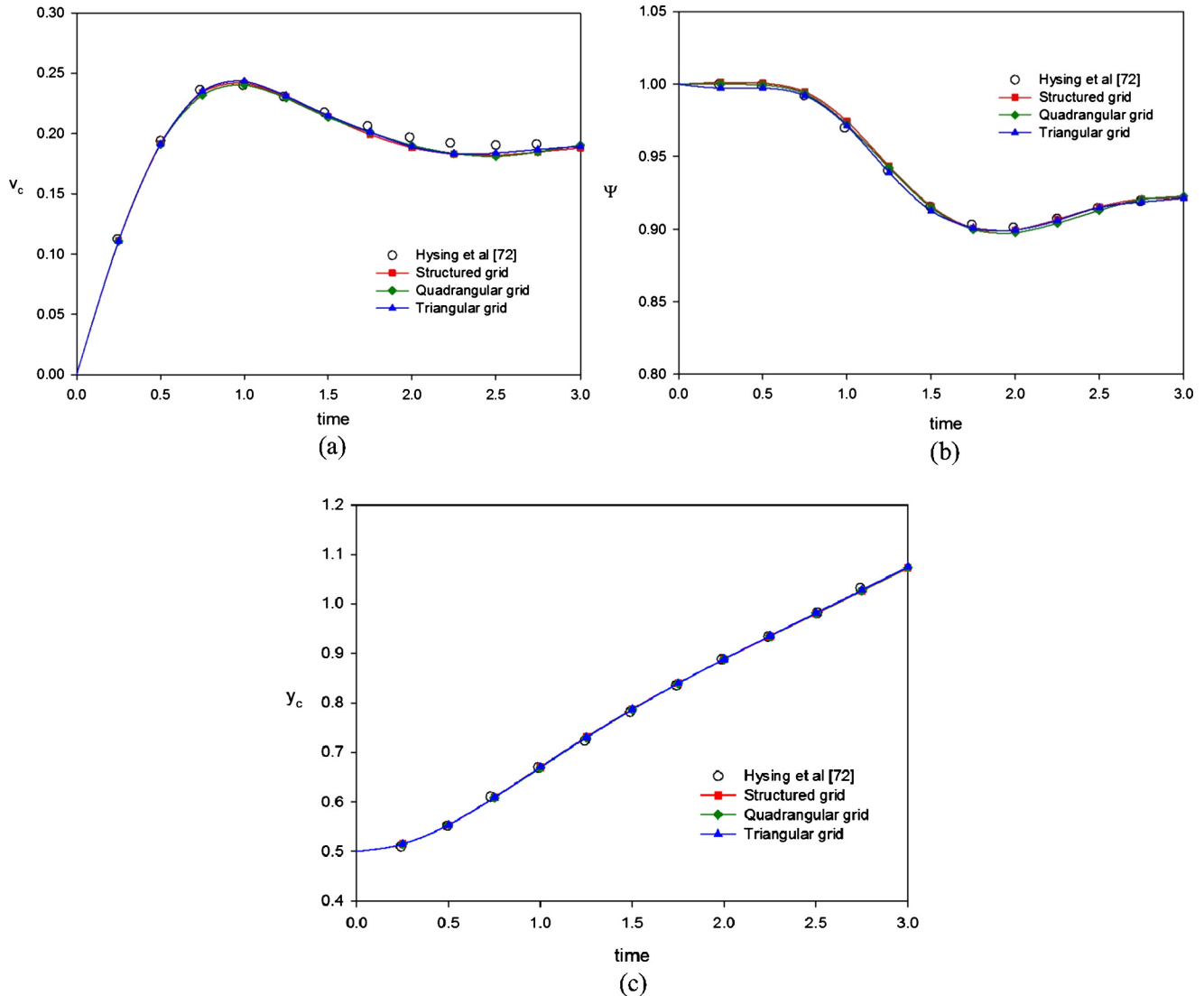


Fig. 11. Rising gas bubble: Time evolution of (a) rise velocity (b) circularity and (c) center of mass.

Table 5

Liquid and vapor properties for water at near critical conditions [38] ($\sigma = 0.07 \text{ mN/m}$, $h_{lv} = 276.4 \text{ kJ/kg}$).

| | $\rho (\text{kg/m}^3)$ | $\mu (\text{mPa s})$ | $k (\text{W/m K})$ | $c_p (\text{kJ/kg K})$ |
|--------|------------------------|----------------------|--------------------|------------------------|
| Liquid | 402.4 | 0.0467 | 0.5454 | 218 |
| Vapor | 242.7 | 0.0324 | 0.5383 | 352 |

$$Nu = \frac{\lambda_o}{(T_w - T_{sat})} \frac{\partial T}{\partial y} \Big|_w \quad (33)$$

$$\overline{Nu_L} = \frac{1}{L} \int_0^L Nu dx \quad (34)$$

Here $L = \lambda_d/2$ is the length of the heated plate. The time averaged Nusselt number is obtained as:

$$\overline{Nu_T} = \frac{1}{T} \int_0^T \overline{Nu_L} dt \quad (35)$$

A grid independence study was carried out with structured grid sizes of 64×128 , 96×192 and 128×256 . With the three grid sizes considered, the time-averaged Nusselt number is obtained

as 5.08, 5.18 and 5.23 respectively. It is observed that the difference in results with the medium and finest mesh is very less. The results with grid size $\lambda_d/256$ are presented subsequently.

Fig. 12 shows the bubble formation and release pattern with a superheat of 5 K. At the onset, a vapor bulge at the node ($x = 0$) is formed which subsequently grows in size. This vapor mass rises due to the buoyancy force and is connected to the film near the wall by a vapor column. The neck of the vapor column is continuously stretched leading to pinch-off of a vapor bubble. The pinch-off occurs when the bubble is nearly at the location $y = \lambda_d/2$, which is in agreement with other studies [28,38,74,75]. The remaining vapor recoils back due to capillary forces and collapses into the film near the wall. This initiates an interfacial wave motion from the node towards the antinode, which can be seen clearly in Fig. 12 from time $t = 1.155 \text{ s}$ to $t = 1.2 \text{ s}$. Eventually, the film thickness becomes maximum at the antinodes leading to bubble release from these locations. This cycle is observed to repeat periodically with location of bubble release at node and antinode, alternatively.

Fig. 13 shows the temperature field just before the pinch-off of the vapor bubble. The temperature distribution from Lee et al. [75], who used a level set based method for phase change problems, is also presented alongside showing a similar structure of the entire vapor mass before pinch-off. A higher temperature is observed at

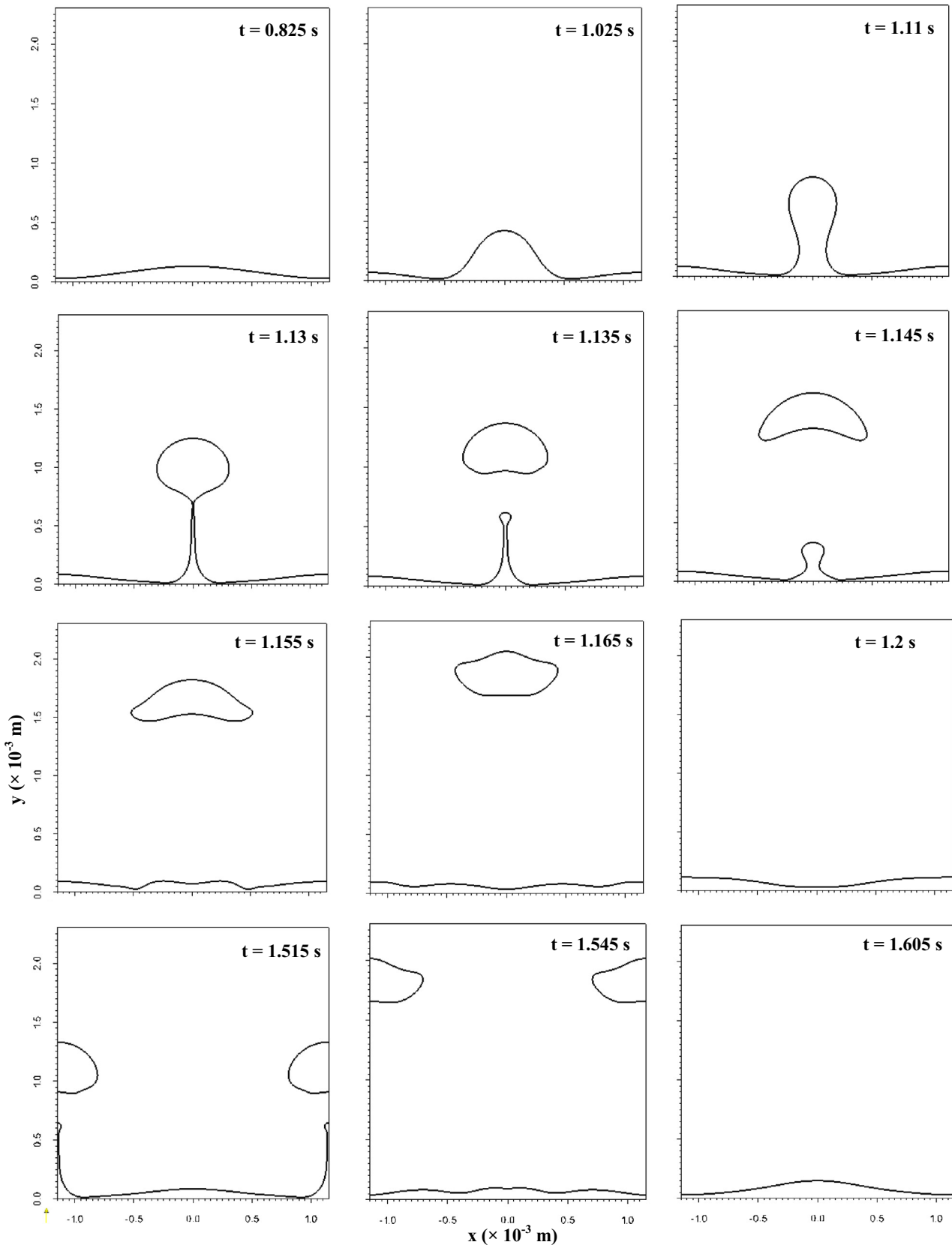


Fig. 12. Bubble release pattern for water at near critical conditions (superheat $\Delta T = 5 \text{ K}$) with 128×256 structured grid.

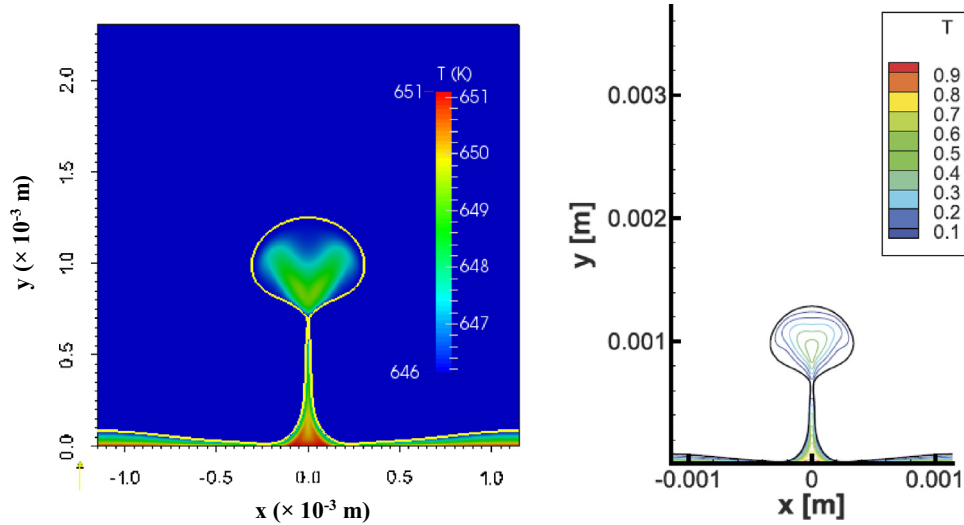


Fig. 13. Temperature field before first bubble pinch-off for water at near critical conditions (superheat $\Delta T = 5$ K) (a) present CLSVOF method (b) Lee et al. [75] (temperature scaled as $(T - T_{\text{sat}})/\Delta T$).

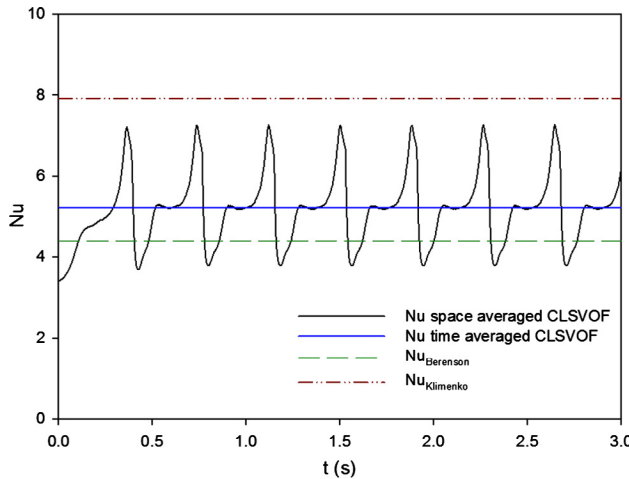


Fig. 14. Nusselt number variation for near critical water at $\Delta T = 5$ K: comparison with semi-empirical correlations of Berenson [76] and Klimenko [77] (correlation values are based on thermodynamic properties at saturation temperature).

the base of the vapor column and the locations of maximum film thickness, while a lower temperature in the region of minimum film thickness shows that the maximum heat transfer takes place at this location.

Fig. 14 shows the variation of space-averaged Nusselt number with time. The periodic variation shows a quasi-steady nature of film boiling. The time-averaged Nusselt number is obtained as 5.23. The Nusselt number obtained from the semi-empirical correlations of Berenson [76] and Klimenko [77] are 4.39 and 7.92 respectively, with the vapor properties being evaluated at the saturation temperature. As reasoned by Son and Dhir [32], the heat transfer predictions from numerical simulations and empirical correlations are better compared with properties evaluated at the same temperature in both cases. The Nusselt number predicted from the present method is found to be bound by the values obtained using the correlations of Berenson [76] and Klimenko [77].

The simulation is also performed using an unstructured quadrangular grid with an equivalent grid size of $\lambda_d/256$. As shown in Fig. 15, a few rows of uniform cells near the wall are considered

while the rest of the domain is discretized with unstructured quadrangular cells. The interface morphology is shown in Fig. 15 at different time instants, which is very similar to as discussed earlier for the case of structured grid. The time-averaged Nusselt number obtained with the unstructured grid is 5.22 which is almost the same as the earlier calculated value using a structured grid. These results show that the present CLSVOF method along with the phase change model is capable of handling phase change problems on unstructured grids. Further, in Table 6, the Nusselt number for the present case obtained from different numerical studies and semi-empirical correlations is compared. Tomar [74] used an operator split CLSVOF method, while the others used level set based methods with structured grids. It can be seen that the present numerical results are in excellent agreement with the results available in the literature.

3.3.2. Film boiling over a horizontal cylinder

Having established the performance of the present CLSVOF method for flat plate geometry on both structured and unstructured grids, natural convection film boiling over a cylinder is studied in this section. Many studies of the direct numerical simulations for boiling flows carried out till date have focused on structured grids. Thus film boiling over a cylinder is not as extensively studied as the case of film boiling on a flat plate. Esmaeeli and Tryggvason [78] extended the front tracking method in conjunction with an immersed boundary method to simulate film boiling on horizontal cylinders. Later, Son and Dhir [31] studied film boiling on a cylinder using an Eulerian grid with a level set/ghost fluid method. Son and Dhir [32] extended their level set based finite difference method to simulate three-dimensional film boiling on a cylinder. The Volume of fluid (or CLSVOF) based methods, although inherently mass-preserving, have to deal with complex geometric procedures for interface reconstruction, advection, and redistancing of the level set function. In particular, the geometric operations for non-orthogonal and unstructured grids are difficult to implement. Recently, Tsui et al. [23] studied film boiling of water at near critical conditions over a cylinder using a volume of fluid method.

The case studied by Tsui et al. [23] is considered in the present study. Water at the same conditions (21.9 MPa, 646 K) is considered as in the previous section. The cylinder diameter, D is 0.211 mm, which is equal to the characteristic length scale

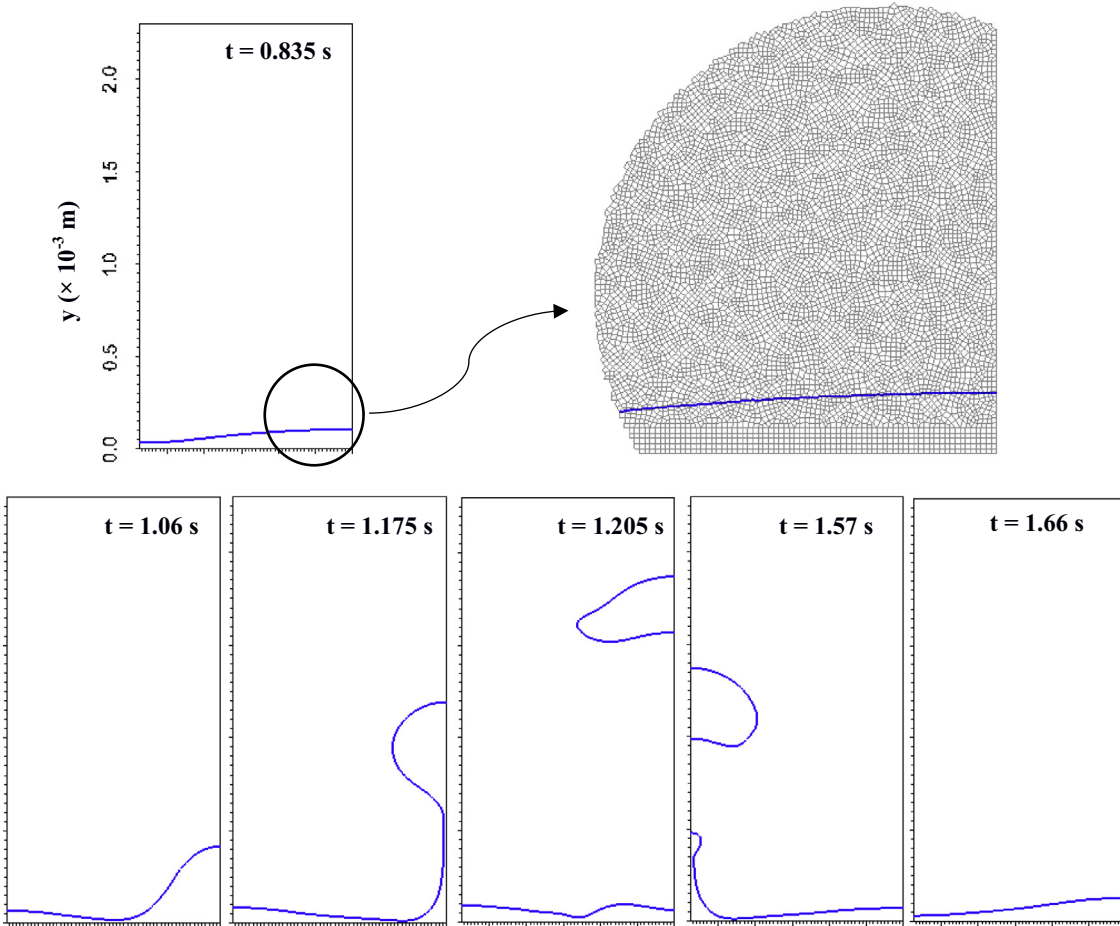


Fig. 15. Bubble release pattern for water at near critical conditions (superheat $\Delta T = 5 \text{ K}$) with unstructured quadrangular grid (grid size $h = \lambda_d/256$).

Table 6

Comparison of heat transfer results for saturated film boiling over a horizontal flat plate.

| | Nusselt number (time-averaged) |
|--------------------------------------------------------|--------------------------------|
| <i>Numerical results</i> | |
| Present CLSVOF method (structured grid) | 5.23 |
| Present CLSVOF method (unstructured quadrangular grid) | 5.22 |
| Gada and Sharma [28] | 5.42 |
| Son and Dhir [30] | 5.58 |
| Tomar [74] (CLSVOF operator split) | 5.06 |
| Lee et al. [75] | 5.1 |
| <i>Semi-empirical correlations</i> | |
| Berenson [76] | 4.39 |
| Klimenko [77] | 7.92 |

(Correlation values are based on thermodynamic properties at saturation temperature).

$(\lambda_o = \sqrt{\sigma/(\rho_l - \rho_v)g})$ of the problem. The cylinder is placed at $(3.5D, 3.5D)$ in a computational domain of $7D \times 15D$. Owing to the symmetry of the problem, only half of the domain ($3.5D \times 15D$) is considered for the computation.

No slip boundary condition is specified at the cylinder surface, while slip condition is used at the other boundaries. Outflow boundary condition is used at the top boundary of the domain. The temperature at the cylinder wall is specified as $T_w = T_{sat} + \Delta T$, where ΔT is the wall superheat and T_{sat} is the saturation temperature. In the present study, results are presented for the wall superheats of 5 K, 10 K and 20 K. A vapor film blankets the cylinder

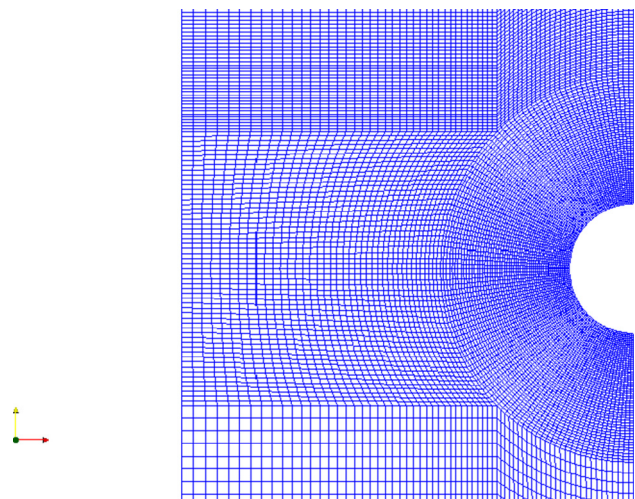


Fig. 16. Computational mesh used for film boiling over a horizontal cylinder.

wall from the saturated liquid and the film thickness is initialized uniformly as $0.1 D$ around the cylinder. As in the previous case of film boiling over a flat plate, the initial velocity field in the domain is specified as zero, while for the temperature a linear variation from the wall temperature to the saturated liquid temperature is initialized in the vapor phase. Based on a grid sensitivity test, a mesh with 22,112 cells is used in the present study. The mesh layout is shown in Fig. 16 and it can be seen that the density of the

cells is kept maximum near the cylinder. The grid spacing is non-uniform near the cylinder as well as in other parts of the domain. Simulations were carried out for each wall superheat till periodicity in bubble release or formation of a stable vapor column (at higher ΔT) is established.

The heat transfer results are quantitatively presented in terms of Nusselt number. The local Nusselt number (Nu_D) and the space-averaged Nusselt number \bar{Nu}_D at the heated cylinder wall are given as:

$$Nu_D = \frac{D}{(T_w - T_{sat})} \frac{\partial T}{\partial n} \Big|_w \quad (36)$$

where n represents the direction normal to the cylinder wall.

$$\bar{Nu}_D = \frac{1}{2\pi} \int_0^{2\pi} Nu d\theta \quad (37)$$

The time-averaged Nusselt number is calculated as per Eq. (34).

Fig. 17 shows the bubble formation and release pattern for the present case with the wall superheat of 5 K. Initially, the vapor film grows in the upper region of the cylinder, while a thin film sustains around the lower portion of the cylinder and prevents it from collapsing. Similar to the planar film boiling on a flat plate, the vapor mass rises under the action of buoyancy, and a bubble is eventually pinched-off following the stretching and necking of the vapor column connecting it to the film near the cylindrical wall. The recoil of the remaining vapor initiates an interfacial wave motion. The wave causes a back and forth motion of the vapor film around the cylindrical wall (time $t = 0.68$ s to $t = 0.6925$ s in **Fig. 17**), finally stabilizing to initiate another cycle of bubble formation and release. The interface evolution for a superheat of 10 K is shown in **Fig. 18**.

The vapor release pattern is again observed to be periodic and quite similar to the case of 5 K superheat. However, the length of the vapor column is larger leading to bubble pinch-off at a greater distance from the cylinder wall. The film around the cylinder is visibly thicker, while time period of the periodic ebullition cycle is reduced. For a superheat of 20 K, the higher superheat leads to the formation of a stable vapor jet as shown in **Fig. 19**. The vapor column continues to elongate without pinch-off and a continuous infusion of vapor through this column leads to the stable vapor jet structure.

Fig. 20 shows the variation of space-averaged Nusselt number with time for different wall superheats. For the wall superheats of 5 K and 10 K, the variation of the space-averaged Nusselt number is periodic as anticipated from the periodic interface evolution cycle discussed in preceding paragraph. For the wall superheat of 20 K, the Nusselt number becomes constant after the formation of a stable vapor jet. The time-averaged Nusselt number values are also shown in **Fig. 20** and further compared in **Table 7** with the numerical results of Tsui et al. [23] and correlation of Bromley [79]. Bromley [79] developed a semi-empirical correlation for film boiling heat transfer over a cylinder as:

$$\bar{Nu}_D = 0.62(Gr Pr_v/Ja_v^*)^{1/4} \quad (38)$$

where the constant 0.62 was determined experimentally. The other parameters appearing in the correlation are given as:

$$Grashof number Gr = \frac{\rho_v(\rho_l - \rho_v)gD^3}{\mu_v^2} \quad (39)$$

$$Prandtl number Pr = \frac{\mu_v C_{pv}}{k_v} \quad (40)$$

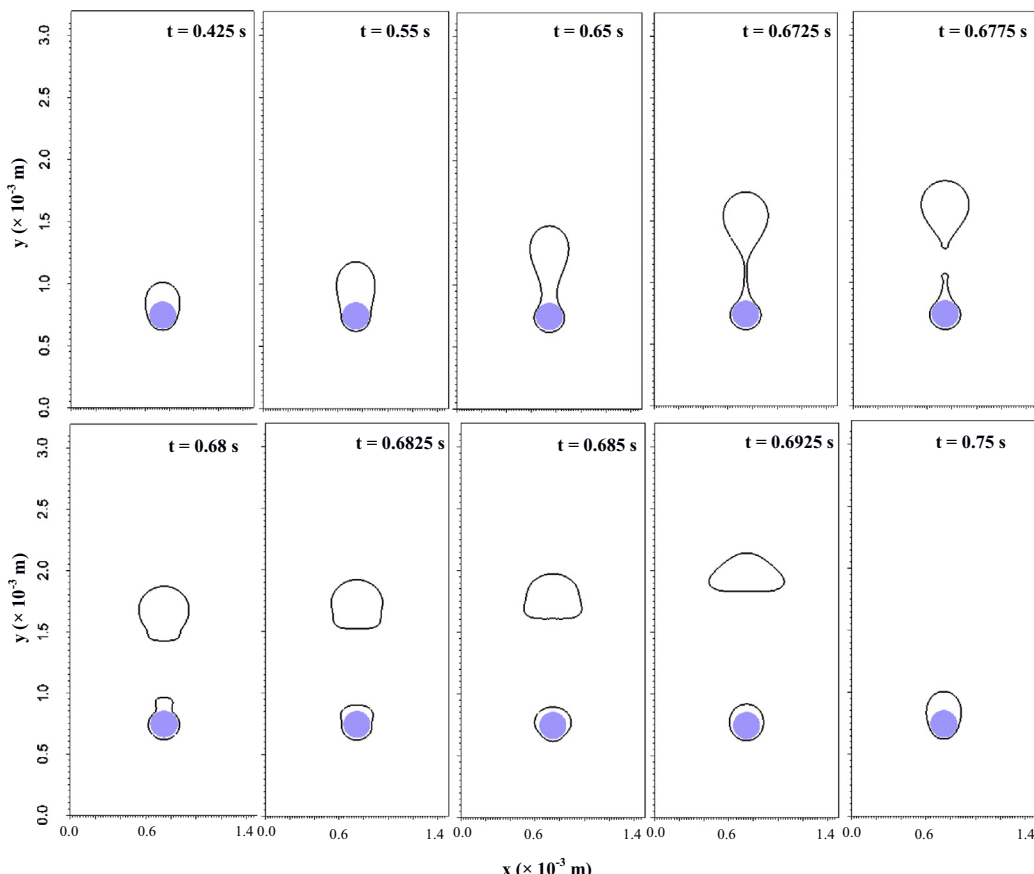


Fig. 17. Bubble release pattern for water at near critical conditions (superheat $\Delta T = 5$ K) over a horizontal cylinder.

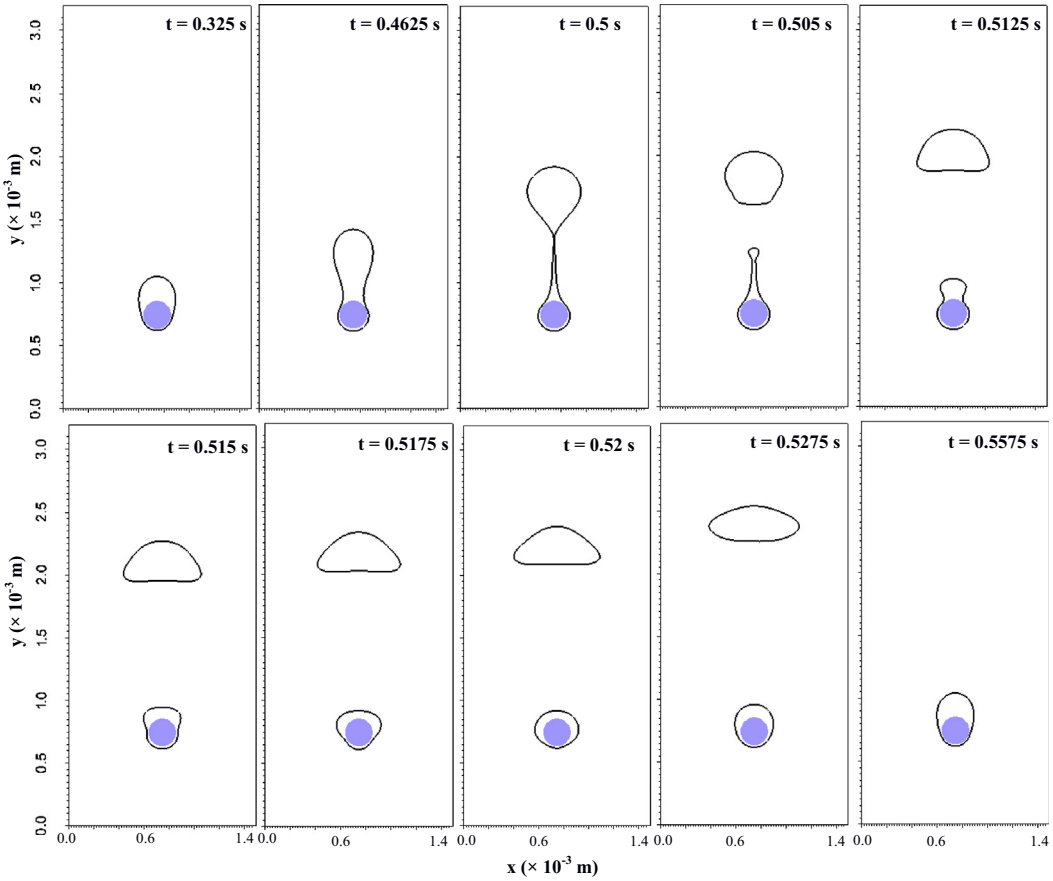


Fig. 18. Bubble release pattern for water at near critical conditions (superheat $\Delta T = 10$ K) over a horizontal cylinder.

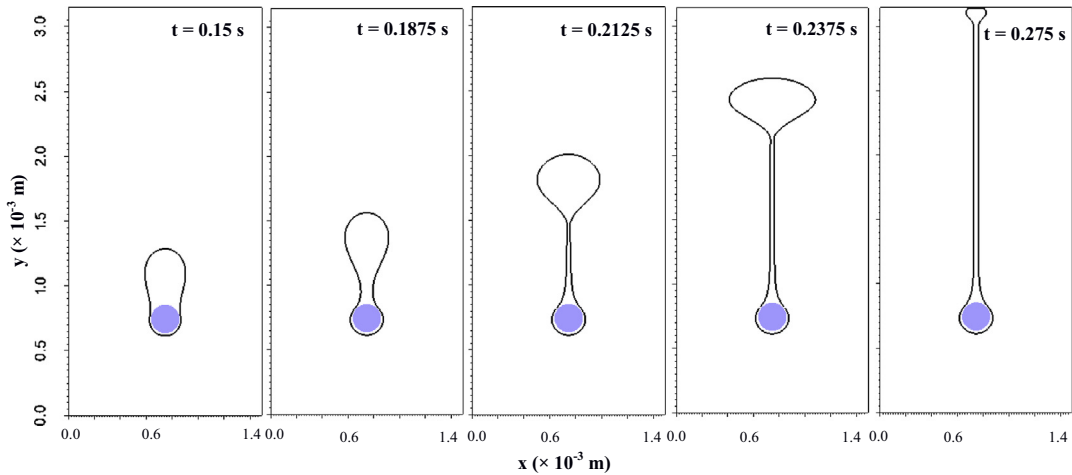


Fig. 19. Interface morphology for water at near critical conditions (superheat $\Delta T = 20$ K) over a horizontal cylinder: formation of vapor jet.

$$\text{Modified Jacob number } Ja_v^* = \frac{Ja_v}{1 + 0.34Ja_v} \quad (41)$$

$$\text{Jacob number } Ja_v = \frac{c_{pv}\Delta T}{h_{lv}} \quad (42)$$

As can be seen from Table 7, the values obtained by Tsui et al. [23] using a VOF method show a significant deviation from the values obtained using Bromley's correlation, while the results obtained with the present CLSVOF method show a much better agreement. As discussed in other studies [23,73,75], one of the rea-

sons for deviation of the numerical results from the correlation values can be attributed to the consideration of constant fluid properties in numerical simulations. Another factor can be the several underlying assumptions in the theory from which the correlations are deduced. Differences in the numerical and correlation predictions have also been observed in the heat transfer results for film boiling over a cylinder by Esmaeeli and Tryggvason [78]. Considering all the above factors, the current numerical results show a very good agreement with the semi-empirical correlation of Bromley [79] as compared to the results reported by Tsui et al. [23] with a VOF method.

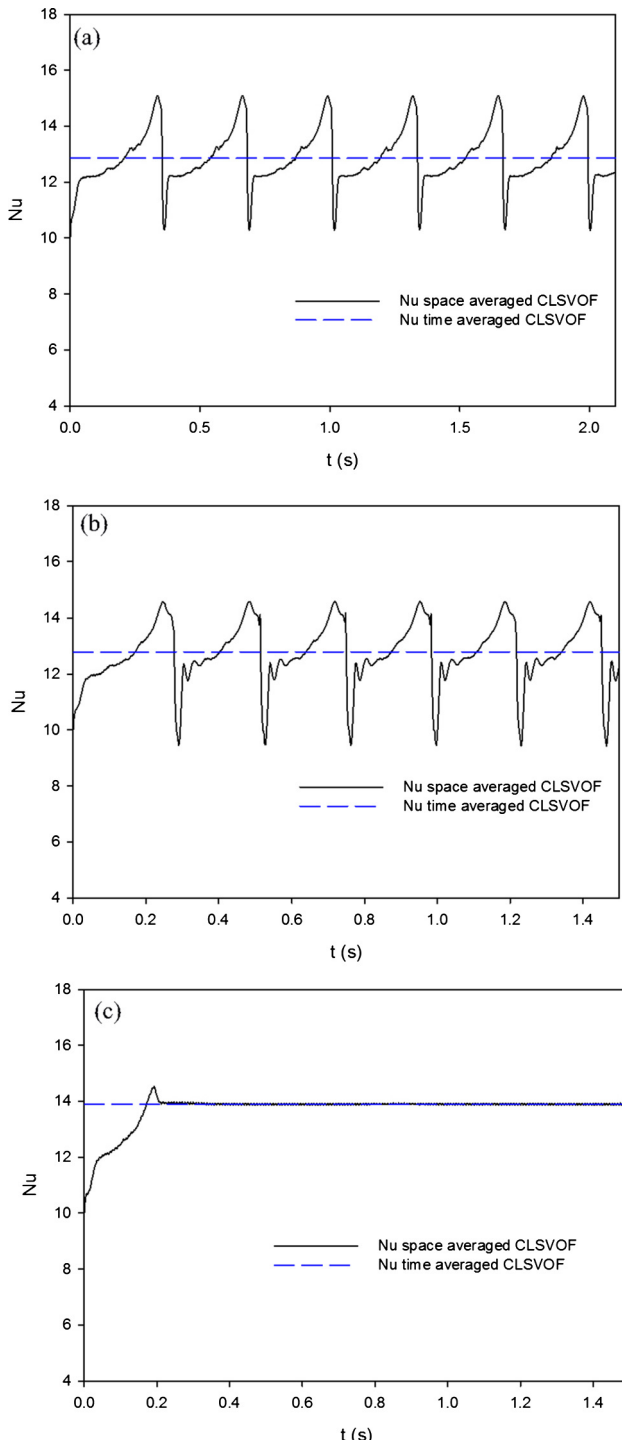


Fig. 20. Nusselt number variation for natural convection film boiling over a horizontal cylinder: water at near critical conditions (a) $\Delta T = 5\text{ K}$ (b) $\Delta T = 10\text{ K}$ (c) $\Delta T = 20\text{ K}$.

Table 7

Comparison of heat transfer results for film boiling over a cylinder (time-averaged Nusselt number).

| | 5 K | 10 K | 20 K |
|-----------------------------|-------|-------|-------|
| Present CLSVOF method | 12.86 | 12.78 | 13.89 |
| Bromley [79] | 8.53 | 8.17 | 7.97 |
| Tsui et al. [23] VOF method | – | 23.3 | 24.6 |

(Correlation values are calculated based on thermodynamic properties at saturation temperature).

4. Conclusions

Based on the literature review, it was identified that a direct extension of CLSVOF method implemented for structured grids has not been attempted for unstructured grids including phase change. In the few studies that coupled the volume of fluid and the level set methods for two-phase flows without phase change on unstructured grids, a detailed quantitative validation of the method with both advection and two-phase flow tests has not been carried out.

In this study, a CLSVOF method is developed for unstructured grids to perform direct numerical simulations of two-phase flows including phase change. A two-phase flow solver incorporating phase change model is developed for collocated unstructured grids. For the volume fraction advection, flux polygons are constructed using vertex velocities to simplify this step in terms of complexity and cost. A scaling factor based on cell face velocities is used to correct the advected volume fraction. The level set field is advected using a TVD scheme and geometrically reinitialized at the end of each time step.

Prior to simulation of film boiling, the method is validated extensively, both qualitatively as well as quantitatively, for a number of advection test cases and two-phase problems. The results are presented for structured, unstructured quadrangular and unstructured triangular grids, to fully assess the performance of the present CLSVOF method for the interface reconstruction and advection, and the surface tension modelling.

- For the advection test cases of simple translation, Zalesak slotted disk rotation, and single vortex flow, the results obtained with the present CLSVOF method for structured and unstructured grids using the PLIC interface reconstruction, in terms of interface shape and error norms, compared very well with those available in literature using higher order interface reconstruction on structured grids and adaptive meshes.
- Static liquid drop, Rayleigh-Taylor instability and rising gas bubble problems were considered for the validation of two-phase flow solver. The interface morphology as well as other benchmark quantities calculated for these problems with the structured and the unstructured grids are in excellent agreement with previous studies, establishing the accuracy of the surface tension modelling in the present CLSVOF framework.
- For saturated film boiling on a horizontal flat plate, simulations were carried out on structured as well as unstructured grids. The interface evolution and heat transfer results show excellent agreement with other numerical results available in the literature using structured grids.
- The numerical study of natural convection film boiling over a horizontal cylinder with present CLSVOF method at different wall superheats shows a better agreement with semi-empirical correlations compared to available numerical results with a volume of fluid method for unstructured grids.

Conflict of interest

Authors declare that there is no conflict of interest.

Appendix A. Supplementary material

Supplementary data associated with this article can be found, in the online version, at <https://doi.org/10.1016/j.ijheatmasstransfer.2018.01.091>.

References

- G. Son, V.K. Dhir, Numerical simulation of saturated film boiling on a horizontal surface, ASME J. Heat Transf. 119 (1997) 525–533.

- [2] D. Juric, G. Tryggvason, Computations of boiling flows, *Int. J. Multiph. Flow* 24 (3) (1998) 387–410.
- [3] S.W. Welch, J. Wilson, A volume of fluid based method for fluid flows with phase change, *J. Comput. Phys.* 160 (2) (2000) 662–682.
- [4] D. Lakehal, M. Meier, M. Fulgosi, Interface tracking towards the direct simulation of heat and mass transfer in multiphase flows, *Int. J. Heat Fluid Flow* 23 (3) (2002) 242–257.
- [5] S.O. Unverdi, G. Tryggvason, A front-tracking method for viscous, incompressible, multi-fluid flows, *J. Comput. Phys.* 100 (1) (1992) 25–37.
- [6] D.L. Youngs, Time-dependent multi-material flow with large fluid distortion, in: K.W. Morton, M.J. Baines (Eds.), *Numerical Methods For Fluid Dynamics*, Academic Press, New York, NY, USA, 1982, pp. 273–285.
- [7] J.E. Pilled, An Analysis of Piecewise Linear Interface Reconstruction Algorithms for Volume-of-fluid Methods (MS thesis), University of California, Davis, 1992.
- [8] Y. Renardy, M. Renardy, PROST: a parabolic reconstruction of surface tension for the volume-of-fluid method, *J. Comput. Phys.* 183 (2) (2002) 400–421.
- [9] J. López, J. Hernández, P. Gómez, F. Faura, A volume of fluid method based on multidimensional advection and spline interface reconstruction, *J. Comput. Phys.* 195 (2) (2004) 718–742.
- [10] S.V. Diwakar, S.K. Das, T. Sundararajan, A quadratic spline based interface (QUASI) reconstruction algorithm for accurate tracking of two-phase flows, *J. Comput. Phys.* 228 (24) (2009) 9107–9130.
- [11] S.J. Cummins, M.M. Francois, D.B. Kothe, Estimating curvature from volume fractions, *Comput. Struct.* 83 (6) (2005) 425–434.
- [12] M.M. Francois, S.J. Cummins, E.D. Dendy, D.B. Kothe, J.M. Sicilian, M.W. Williams, A balanced-force algorithm for continuous and sharp interfacial surface tension models within a volume tracking framework, *J. Comput. Phys.* 213 (1) (2006) 141–173.
- [13] S. Popinet, An accurate adaptive solver for surface-tension-driven interfacial flows, *J. Comput. Phys.* 228 (16) (2009) 5838–5866.
- [14] T. Abadie, J. Aubin, D. Legendre, On the combined effects of surface tension force calculation and interface advection on spurious currents within Volume of Fluid and Level Set frameworks, *J. Comput. Phys.* 297 (2015) 611–636.
- [15] K. Ito, T. Kunugi, S. Ohno, H. Kamide, H. Ohshima, A high-precision calculation method for interface normal and curvature on an unstructured grid, *J. Comput. Phys.* 273 (2014) 38–53.
- [16] C.B. Ivey, P. Moin, Accurate interface normal and curvature estimates on three-dimensional unstructured non-convex polyhedral meshes, *J. Comput. Phys.* 300 (2015) 365–386.
- [17] S.H. Garrioch, B.R. Baliga, A PLIC volume tracking method for the simulation of two-fluid flows, *Int. J. Numer. Meth. Fluids* 52 (10) (2006) 1093–1134.
- [18] Z. Wang, A.Y. Tong, A sharp surface tension modeling method for two-phase incompressible interfacial flows, *Int. J. Numer. Meth. Fluids* 64 (7) (2010) 709–732.
- [19] W.J. Rider, D.B. Kothe, Reconstructing volume tracking, *J. Comput. Phys.* 141 (2) (1998) 112–152.
- [20] J. Hernández, J. López, P. Gómez, C. Zanzi, F. Faura, A new volume of fluid method in three dimensions—Part I: multidimensional advection method with face-matched flux polyhedral, *Int. J. Numer. Meth. Fluids* 58 (8) (2008) 897–921.
- [21] C.R. Kharangate, I. Mudawar, Review of computational studies on boiling and condensation, *Int. J. Heat Mass Transf.* 108 (2017) 1164–1196.
- [22] Y.Y. Tsui, S.W. Lin, A VOF-based conservative interpolation scheme for interface tracking (CISIT) of two-fluid flows, *Numer. Heat Transf. Part B: Fundam.* 63 (4) (2013) 263–283.
- [23] Y.Y. Tsui, S.W. Lin, Y.N. Lai, F.C. Wu, Phase change calculations for film boiling flows, *Int. J. Heat Mass Transf.* 70 (2014) 745–757.
- [24] Y.Y. Tsui, S.W. Lin, Three-dimensional modeling of fluid dynamics and heat transfer for two-fluid or phase change flows, *Int. J. Heat Mass Transf.* 93 (2016) 337–348.
- [25] S.T. Ding, B. Luo, G. Li, A volume of fluid based method for vapor-liquid phase change simulation with numerical oscillation suppression, *Int. J. Heat Mass Transf.* 110 (2017) 348–359.
- [26] S. Osher, J.A. Sethian, Fronts propagating with curvature-dependent speed: algorithms based on Hamilton-Jacobi formulations, *J. Comput. Phys.* 79 (1) (1988) 12–49.
- [27] M. Sussman, P. Smereka, S. Osher, A level set approach for computing solutions to incompressible two-phase flow, *J. Comput. Phys.* 114 (1) (1994) 146–159.
- [28] V.H. Gada, A. Sharma, On a novel dual-grid level-set method for two-phase flow simulation, *Numer. Heat Transf. Part B: Fundam.* 59 (1) (2011) 26–57.
- [29] R.P. Fedkiw, T. Aslam, B. Merriman, S. Osher, A non-oscillatory Eulerian approach to interfaces in multimaterial flows (the ghost fluid method), *J. Comput. Phys.* 152 (2) (1999) 457–492.
- [30] G. Son, V.K. Dhir, Numerical simulation of film boiling near critical pressures with a level set method, *ASME J. Heat Transf.* 120 (1998) 183–192.
- [31] G. Son, V.K. Dhir, A level set method for analysis of film boiling on an immersed solid surface, *Numer. Heat Transf. Part B: Fundam.* 52 (2) (2007) 153–177.
- [32] G. Son, V.K. Dhir, Three-dimensional simulation of saturated film boiling on a horizontal cylinder, *Int. J. Heat Mass Transf.* 51 (5) (2008) 1156–1167.
- [33] A. Bourlioux, A coupled level-set volume-of-fluid algorithm for tracking material interfaces, in: Proceedings of the 6th International Symposium on Computational Fluid Dynamics, Lake Tahoe, CA, vol. 15, September 1995.
- [34] M. Sussman, E.G. Puckett, A coupled level set and volume-of-fluid method for computing 3D and axisymmetric incompressible two-phase flows, *J. Comput. Phys.* 162 (2) (2000) 301–337.
- [35] G. Son, N. Hur, A coupled level set and volume-of-fluid method for the buoyancy-driven motion of fluid particles, *Numer. Heat Transf.: Part B: Fundam.* 42 (6) (2002) 523–542.
- [36] M. Sussman, A second order coupled level set and volume-of-fluid method for computing growth and collapse of vapor bubbles, *J. Comput. Phys.* 187 (1) (2003) 110–136.
- [37] A.Y. Tong, Z. Wang, A numerical method for capillarity-dominant free surface flows, *J. Comput. Phys.* 221 (2) (2007) 506–523.
- [38] G. Tomar, G. Biswas, A. Sharma, A. Agrawal, Numerical simulation of bubble growth in film boiling using a coupled level-set and volume-of-fluid method, *Phys. Fluids* 17 (11) (2005) 112103.
- [39] D. Gerlach, G. Tomar, G. Biswas, F. Durst, Comparison of volume-of-fluid methods for surface tension-dominant two-phase flows, *Int. J. Heat Mass Transf.* 49 (3) (2006) 740–754.
- [40] B.M. Ningegowda, B. Premachandran, A Coupled Level Set and Volume of Fluid method with multi-directional advection algorithms for two-phase flows with and without phase change, *Int. J. Heat Mass Transf.* 79 (2014) 532–550.
- [41] S.W. Welch, G. Biswas, Direct simulation of film boiling including electrohydrodynamic forces, *Phys. Fluids* 19 (1) (2007) 012106.
- [42] G. Tomar, G. Biswas, A. Sharma, S.W.J. Welch, Influence of electric field on saturated film boiling, *Phys. Fluids* 21 (3) (2009) 032107.
- [43] X. Yang, A.J. James, J. Lowengrub, X. Zheng, V. Cristini, An adaptive coupled level-set/volume-of-fluid interface capturing method for unstructured triangular grids, *J. Comput. Phys.* 217 (2) (2006) 364–394.
- [44] B.M. Ningegowda, B. Premachandran, Numerical investigation of the pool film boiling of water and R134a over a horizontal surface at near-critical conditions, *Numer. Heat Transf. Part A: Appl.* 71 (1) (2017) 44–71.
- [45] N. Balcázar, O. Lehmkuhl, L. Jofre, J. Rigola, A. Oliva, A coupled volume-of-fluid/level-set method for simulation of two-phase flows on unstructured meshes, *Comput. Fluids* 124 (2016) 12–29.
- [46] D.L. Sun, W.Q. Tao, A coupled volume-of-fluid and level set (VOSET) method for computing incompressible two-phase flows, *Int. J. Heat Mass Transf.* 53 (4) (2010) 645–655.
- [47] D.Z. Guo, D.L. Sun, Z.Y. Li, W.Q. Tao, Phase change heat transfer simulation for boiling bubbles arising from a vapor film by the VOSET method, *Numer. Heat Transf. Part A: Appl.* 59 (11) (2011) 857–881.
- [48] K. Ling, Z.H. Li, D.L. Sun, Y.L. He, W.Q. Tao, A three-dimensional volume of fluid & level set (VOSET) method for incompressible two-phase flow, *Comput. Fluids* 118 (2015) 293–304.
- [49] Z. Cao, D. Sun, B. Yu, J. Wei, A coupled volume-of-fluid and level set (VOSET) method based on remapping algorithm for unstructured triangular grids, *Int. J. Heat Mass Transf.* 111 (2017) 232–245.
- [50] I.R. Park, K.S. Kim, J. Kim, S.H. Van, A volume-of-fluid method for incompressible free surface flows, *Int. J. Numer. Meth. Fluids* 61 (12) (2009) 1331–1362.
- [51] M. Haghshenas, J.A. Wilson, R. Kumar, Algebraic coupled level set-volume of fluid method for surface tension dominant two-phase flows, *Int. J. Multiph. Flow* 90 (2017) 13–28.
- [52] A. Albadawi, D.B. Donoghue, A.J. Robinson, D.B. Murray, Y.M.C. Delauré, Influence of surface tension implementation in volume of fluid and coupled volume of fluid with level set methods for bubble growth and detachment, *Int. J. Multiph. Flow* 53 (2013) 11–28.
- [53] A. Ferrari, M. Magnini, J.R. Thome, A Flexible Coupled Level Set and Volume of Fluid (flexCLF) method to simulate microscale two-phase flow in non-uniform and unstructured meshes, *Int. J. Multiph. Flow* 91 (2017) 276–295.
- [54] Y.Y. Tsui, C.Y. Liu, S.W. Lin, Coupled level-set and volume-of-fluid method for two-phase flow calculations, *Numer. Heat Transf. Part B: Fundam.* 71 (2) (2017) 173–185.
- [55] S.W. Welch, T. Rachidi, Numerical computation of film boiling including conjugate heat transfer, *Numer. Heat Transf.: Part B: Fundam.* 42 (1) (2002) 35–53.
- [56] J.U. Brackbill, D.B. Kothe, C. Zemach, A continuum method for modeling surface tension, *J. Comput. Phys.* 100 (2) (1992) 335–354.
- [57] J. López, J. Hernández, Analytical and geometrical tools for 3D volume of fluid methods in general grids, *J. Comput. Phys.* 227 (12) (2008) 5939–5948.
- [58] P. Liovic, M. Rudman, J.L. Liow, D. Lakehal, D. Kothe, A 3D unsplit-advection volume tracking algorithm with planarity-preserving interface reconstruction, *Comput. Fluids* 35 (10) (2006) 1011–1032.
- [59] L. Jofre, O. Lehmkuhl, J. Castro, A. Oliva, A 3-D Volume-of-Fluid advection method based on cell-vertex velocities for unstructured meshes, *Comput. Fluids* 94 (2014) 14–29.
- [60] M.S. Darwish, F. Moulkalled, TVD schemes for unstructured grids, *Int. J. Heat Mass Transf.* 46 (4) (2003) 599–611.
- [61] T. Lehnhäuser, M. Schäfer, Improved linear interpolation practice for finite-volume schemes on complex grids, *Int. J. Numer. Meth. Fluids* 38 (7) (2002) 625–645.
- [62] L. Sun, S.R. Mathur, J.Y. Murthy, An unstructured finite-volume method for incompressible flows with complex immersed boundaries, *Numer. Heat Transf. Part B: Fundam.* 58 (4) (2010) 217–241.
- [63] S. Patankar, *Numerical Heat Transfer and Fluid Flow*, CRC Press, 1980.
- [64] E.G. Puckett, A volume-of-fluid interface tracking algorithm with applications to computing shock wave refraction, in: Proceedings of the Fourth International Symposium on Computational Fluid Dynamics, 1991, pp. 933–938.
- [65] S.T. Zalesak, Fully multidimensional flux-corrected transport algorithms for fluids, *J. Comput. Phys.* 31 (3) (1979) 335–362.

- [66] M. Rudman, Volume-tracking methods for interfacial flow calculations, *Int. J. Numer. Meth. Fluids* 24 (7) (1997) 671–691.
- [67] N. Balcázar, L. Jofré, O. Lehmkuhl, J. Castro, J. Rigola, A finite-volume/level-set method for simulating two-phase flows on unstructured grids, *Int. J. Multiph. Flow* 64 (2014) 55–72.
- [68] J.B. Dupont, D. Legendre, Numerical simulation of static and sliding drop with contact angle hysteresis, *J. Comput. Phys.* 229 (7) (2010) 2453–2478.
- [69] S. Popinet, S. Zaleski, A front-tracking algorithm for accurate representation of surface tension, *Int. J. Numer. Meth. Fluids* 30 (6) (1999) 775–793.
- [70] D. Zuzio, J.L. Estivalezes, An efficient block parallel AMR method for two phase interfacial flow simulations, *Comput. Fluids* 44 (1) (2011) 339–357.
- [71] J. López, J. Hernández, P. Gómez, F. Faura, An improved PLIC-VOF method for tracking thin fluid structures in incompressible two-phase flows, *J. Comput. Phys.* 208 (1) (2005) 51–74.
- [72] S.R. Hysing, S. Turek, D. Kuzmin, N. Parolini, E. Burman, S. Ganesan, L. Tobiska, Quantitative benchmark computations of two-dimensional bubble dynamics, *Int. J. Numer. Meth. Fluids* 60 (11) (2009) 1259–1288.
- [73] D.K. Agarwal, S.W.J. Welch, G. Biswas, F. Durst, Planar simulation of bubble growth in film boiling in near-critical water using a variant of the VOF method, *J. Heat Transf.* 126 (3) (2004) 329–338.
- [74] G. Tomar, Analysis of Interfacial Instabilities in Adhesion, Dewetting and Phase Change (PhD thesis), IIT Kanpur, November 2007.
- [75] M.S. Lee, A. Riaz, V. Aute, Direct numerical simulation of incompressible multiphase flow with phase change, *J. Comput. Phys.* 344 (2017) 381–418.
- [76] P.J. Berenson, Film-boiling heat transfer from a horizontal surface, *J. Heat Transf.* 83 (3) (1961) 351–356.
- [77] V.V. Klimenko, Film boiling on a horizontal plate—new correlation, *Int. J. Heat Mass Transf.* 24 (1) (1981) 69–79.
- [78] A. Esmaeli, G. Tryggvason, A front tracking method for computations of boiling in complex geometries, *Int. J. Multiph. Flow* 30 (7) (2004) 1037–1050.
- [79] L.A. Bromley, Heat transfer in stable film boiling, *Chem. Eng. Progr.* 46 (1950) 221–227.